International Journal of Extreme Manufacturing

TOPICAL REVIEW • OPEN ACCESS

Metal-organic frameworks for gas sensors: comprehensive review from principal, fabrication to application

To cite this article: Soon Hyeong So *et al* 2026 *Int. J. Extrem. Manuf.* **8** 012001

OPEN ACCESS
IMMT | IOP Publishing
International Journal of Extreme Manufacturing
Int. J. Extrem. Manuf. **8** (2026) 012001 (30pp)
https://doi.org/10.1088/2631-7990/ae00a9

Topical Review

Metal-organic frameworks for gas sensors: comprehensive review from principal, fabrication to application

Soon Hyeong So[1,§], Seung Yong Lee[2,§], Hohyung Kang[3,§], Hyegi Min[4], Hee-Tae Jung[3], Kyu Hyoung Lee[2,*] and Dae Woo Kim[1,*]

[1] Department of Chemical and Biomolecular Engineering, YONSEI University, Seoul 03722, Republic of Korea
[2] Department of Material Science and Engineering, YONSEI University, Seoul 03722, Republic of Korea
[3] Korea Advanced Institute of Science Technology, Daejeon 34141, Republic of Korea
[4] Nick J. Holonyak Micro and Nanotechnology Laboratory, University of Illinois at Urbana–Champaign, Urbana, Illinois 61801, United States of America

E-mail: khlee2018@yonsei.ac.kr and audw1105@yonsei.ac.kr

Received 26 September 2024, revised 2 March 2025
Accepted for publication 27 August 2025
Published 15 September 2025

Abstract

Gas sensors are valuable tools for human applications, and extensive research has been conducted in this field. However, practical implementation has yet to be fully realized. In response, efforts have been made to explore metal-organic frameworks (MOFs), a novel class of porous materials, as potential solutions. MOFs exhibit exceptional porosity and highly tunable chemical compositions and structures, giving rise to a wide range of unique physical and chemical properties. Significant progress has been achieved in developing MOF-based gas sensors, improving sensing performance for various gases. This review aims to provide a comprehensive understanding of MOF-based gas sensors, even for readers unfamiliar with MOFs and gas sensors. It covers the working principles of these sensors, fundamental concepts of MOFs, strategies for tuning MOF properties, fabrication techniques for MOF films, and recent studies on MOF and MOF-derivative gas sensors. Finally, current challenges, overlooked aspects, and future directions for fully exploiting the potential of MOFs in gas sensor development are discussed.

Keywords: metal organic framework, gas sensor, gas transport, fabrication, review

§ These authors contributed equally to this work and should be considered co-first-author.
* Authors to whom any correspondence should be addressed.

Abbreviation

MOF	Metal-organic Framework
SMO	Semiconducting Metal-oxide
SBU	Secondary Building Unit
BTC	1,3,5-benzenetricarboxylate
BDC	1,4-benzenedicarboxylate
IRMOF-1	Isoreticular MOF-1
DMF	Dimethylformamide
TMA	Trimesic acid (benzene-1,3,5-tricarboxylic acid)
TGA	Thermal gravimetric analysis
BET	Brunauer–Emmett–Teller
DOBDC	2,5-dioxido-1,4-benzenedicarboxylate
2-MeIM	2-methylimidazolate
IL	Ionic liquid
UiO	Universitetet I Oslo
$\tau 90$	Response speed
$\tau 10$	Recovery time
ppm	Parts per million
ppb	Parts per billion
MFM	Manchester framework material
HKUST-1	Hong Kong University of Science and Technology-1
QCM	Quartz crystal microbalance
SAW	Surface acoustic wave
DMMP	Dimethyl methylphosphonate
KAUST	King Abdullah University of Science and Technology
CCD	Charged coupled device
RI	Refractive index
TCPP	5,10,15,20-tetrakis-(4-carboxyphenyl) porphyrin
HHTP	2,3,6,7,10,11-hexahydroxytriphenylene
HITP	2,3,6,7,10,11-hexaiminotriphenylene
PDMS	Polydimethylsiloxane
3DOM	Three-dimensional ordered microporous
R_{air}	Electrical resistance under air
R_{gas}	Electrical resistance under gas
C_{air}	Capacitance under air
C_{air}	Capacitance under gas
I_{air}	Electrical current under air
I_{gas}	Electrical current under gas
V_{air}	Bias under air
V_{air}	Bias under gas
f_{air}	Frequency current under air
f_{gas}	Frequency current under gas
λ_{air}	Wavelength under air
λ_{gas}	Wavelength under gas
IDEs	Interdigital electrodes
LOD	limit of detection
FETs	Field-effect transistors
MOSFETs	Metal-oxide-semiconductor field-effect transistors
I_{DS}	Output current
V_{DS}	Voltage
V_{GS}	Gate voltages
V_O	Oxygen vacancy
SPR	Surface plasmon resonance
SERS	Surface-enhanced Raman scattering
BAW	Bulk acoustic wave
FBARs	Film bulk acoustic resonators

1. Introduction

Gas sensors are essential for safety, environmental protection, and health across various areas. In industrial applications, sensors are used to detect harmful, flammable, or toxic gases, preventing accidents such as explosions or poisoning (e.g. H_2S, NH_3, SO_2, NO_x, CO_x, and CS_2). In classic industries handling chemicals, oil and gas, and mining, gas sensors are highly effective in monitoring hazardous gases in real-time. Nowadays, there are growing demands to detect signal gas from hydrogen-based infrastructures and Li-ion battery-adopted systems to prevent explosions[1]. For environmental protection, gas sensors can be used to detect pollutants like carbon dioxide, methane, and nitrogen dioxide, helping regulate air quality and track greenhouse gas emissions. In healthcare, gas sensors are used in medical devices to monitor oxygen levels, detect anesthetic gases, and even identify biomarkers in breath that indicate diseases. In addition, volatile organic compounds (VOCs, e.g. hydrocarbons, alcohols, ketones, aldehydes, etc.) have become a severe problem, therefore, detection and removal of VOCs is another emerging area in healthcare applications[2]. Considering the wide use of gas sensors and their growing demands, it becomes important to develop gas sensors with high selectivity, sensitivity, stability, and response/recovery rate, which can be manufactured in scalable and reproducible manners.

Gas sensors can be classified based on measurement methods such as chemiresistors, capacitive, electrochemical, optical, piezoelectric, photoionization, thermal conductivity, gravimetric, and FET-based sensors, each detecting gas concentrations through different physical or chemical interactions. Characteristics of each sensor type are well summarized in other literature[3−12]. Because of its easy working principle and sensor structure, the most popular chemiresistive gas sensors operate based on variations in electrical properties, such as electrical resistance caused by the interaction with gas species. Although various materials including semiconducting metal-oxides (SMOs), conductive polymers, carbon nanomaterials, transition metal dichalcogenides, etc. have been studied in gas sensing[13−15], it has not been reported to show satisfying performance. Representatively, chemiresistor gas sensors have several drawbacks, including low selectivity, which makes it hard to distinguish between gases, and sensitivity to temperature and humidity, leading to inaccurate readings. They also suffer from long-term instability as their sensitivity degrades over time due to contamination or material aging. Additionally, these sensors can have high power consumption, especially when using heated metal oxides, which limits their use in low-power applications. Lastly, most chemiresistors show a slow recovery time after exposure to high gas concentrations, reducing their efficiency for real-time monitoring[16].

MOFs are novel porous and crystalline materials consisting of metal nodes and organic ligands and have gained tremendous attention because they can display numerous physicochemical properties with facile tunability of structures,

chemical compositions, and functionality[17]. Such attributes have attracted researchers in various applications, including gas storage, gas separation, catalysis, drug delivery, etc. Because of the unique interaction properties with gas molecules, MOFs have been paid attention in the research field of gas sensors as well[18,19]. MOFs have strong advantages for gas sensors because of several reasons. Firstly, MOFs' chemical versatility enables the incorporation of different functional groups, tailoring the sensor's response to particular gases, which can increase selectivity. Particularly, this customization can result in changes in physical properties not only for electrical conductivity but also fluorescence, mass, and reflective index, which are used for detection through various methods. MOFs also exhibit good reversibility in gas adsorption, contributing to their long-term stability and reliability in sensor applications. Additionally, MOFs can be combined with other materials to form composites, further enhancing sensor performance.

When using MOFs in gas sensor channels, they can be categorized based on their electrical conductivity into insulating and conducting types. Most MOFs reported to date are insulating, though conducting MOFs are also emerging. Insulating MOFs are beneficial for their high surface area and selectivity but require additional components for signal detection. Conducting MOFs, on the other hand, offer direct electrical responses and high sensitivity but have issues with stability and selectivity. The choice between insulating and conducting MOFs depends on the specific needs of the gas-sensing application. Despite most MOFs being insulators due to their organic linkers, advances in bandgap engineering and the discovery of mechanisms underlying conductive MOFs have spurred efforts to develop new conductive variants[20]. The interaction of gas molecules with MOFs, including redox reactions at metal sites or active organic linkers, and structural changes from gas adsorption, can change the MOFs' intrinsic electrical resistance. This results in low power consumption and eliminates the need for heating since they can operate at room temperature[21].

Conversely, insulating MOFs can be used to detect gas species by measuring variations in their dielectric constant or relative permittivity. This application involves depositing MOFs between interdigitated electrodes to serve as dielectric layers in capacitive gas sensing. Additionally, Field-Effect Transistor (FET) principles can be applied to MOF gas sensors, where variations in the electric field due to applied voltage modulate the current flowing through semiconductors[22]. Because MOFs specialize in capturing gas molecules, the change in mass with adsorbed gas amounts can transduce mechanical response by employing microcantilever, quartz crystal microbalance, surface acoustic wave, and microresonator[23]. Optically detecting gas is also possible by measuring surface plasmon resonance or surface-enhanced Raman scattering[24]. Additionally, MOF can contribute to the enhancement of sensing performance as supportive components, including catalysts, sieving membranes, or hydrophobic-coating materials. Most importantly, MOFs can be coated on semiconducting materials to filter undesired gas molecules, leading to a higher selectivity than neat semiconductors. This method is relatively simple and effective because the response properties of semiconductors and gas separation properties of MOFs can be controllable controlled separately. To achieve the aforementioned gas sensing performance, MOFs have been tuned in diverse ways, and these tailored MOFs can be deposited in various techniques to fabricate MOF films for gas sensing devices, such as drop-casting, tape-casting, spin-coating, template-mediated synthesis, interfacial synthesis, electrochemical deposition, and exfoliation.

Recently, several significant reviews on MOF-based gas sensors have been published. Park et al. focused exclusively on chemiresistive MOF sensors utilizing 2-D conductive MOFs, while Koo et al. also reviewed only chemiresistive MOF sensors[21]. Jo et al. covered various synthesis methods for MOF films and discussed the relationship between MOF characteristics, such as compositions and structures, though their review was limited to chemiresistive sensors[25]. Zhao's group published a comprehensive review addressing diverse MOF-based gas sensors, including chemiresistive, capacitive/impedimetric, field-effect transistor, Kelvin probe-based, mass-sensitive, and optical sensors, with a focus on large-area fabrication methods[26]. Li's group provided an extensive review on gas sensors using MOFs, covering sensing mechanisms but excluding MOF synthesis and film fabrication techniques[27]. This review aims to provide a comprehensive overview of MOF-based gas sensors, building on the insights from previous literature. It begins by explaining the working principles of various MOF gas sensors, such as chemiresistive, capacitive, mass-sensitive, and optical sensors. It then offers a brief description of prototypical MOFs, outlines strategies for tuning MOFs for gas sensing, and discusses the fabrication methods for MOF films. The review highlights the latest advancements in MOFs and MOF derivatives as sensing materials and support components and concludes with a discussion of current challenges and potential solutions. We believe the day will come when MOF gas sensors are commercially available in real-world applications. Specifically, food contamination can generate a myriad of harmful viruses, parasites, or bacteria, and the evolved gas during the contamination can be detected by MOF gas sensors[28]. Additionally, their low cytotoxicity, intrinsic biodegradability, biological affinity, and the compatibility with biomolecules are appealing to biomedical area[29] while their advantages in high selectivity, real-time analysis, and fast response are expected to be useful in monitoring environmental pollution[30]. To visualize the contribution of MOF to gas sensors, a timeline of development of MOF gas sensors is presented in Figure 1.

2. Working principles of gas sensors

2.1. Chemiresistive sensor

The change in electrical resistivity or conductivity due to variations in surface charge carrier density before and after gas molecule adsorption on the surface of SMO is one of the most representative mechanisms in gas sensing[22−26]. This simple mechanism in chemiresistive gas sensors offers various advantages, including ease of integration into devices and

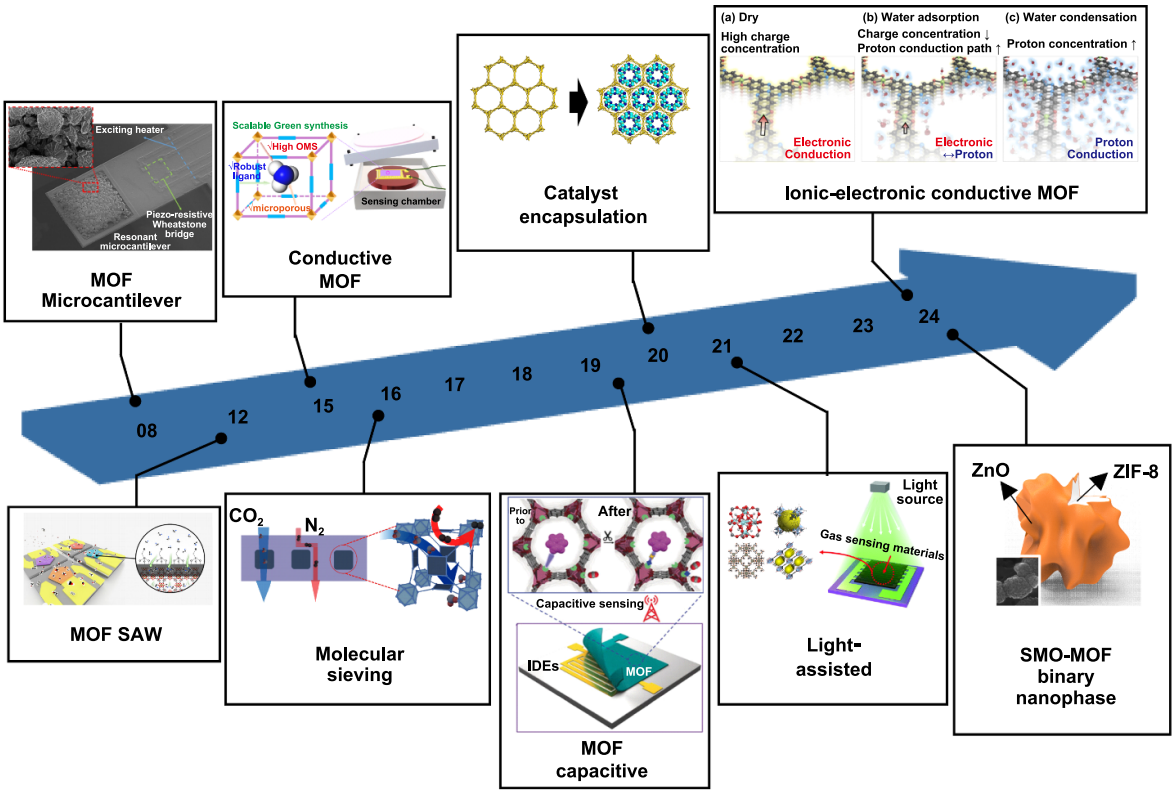

Figure 1. A timeline of development of MOF gas sensors.

low-cost fabrication. When the carrier density increases after gas adsorption on the SMO surface, resistivity decreases due to the formation of a partial charge carrier accumulation region, where the same type of charge carrier from the gas molecules is donated to the SMO surface. Conversely, the formation of larger depletion regions, resulting from the reduction in surface charge carriers or charge recombination between electrons and holes on the SMO surface after gas molecule adsorption, leads to an increase in resistivity. Therefore, the resistivity curve changes depending on the type of gas molecules and the primary conductive carrier type of the MOF. For example, resistivity decreases when exposed to reducing gases in n-type SMOs and to oxidizing gases in p-type SMOs due to major carrier accumulation. On the other hand, resistivity increases when exposed to reducing gases in p-type SMOs and oxidizing gases in n-type SMOs, primarily due to charge recombination and depletion. Thus, a larger difference in electrical resistance in chemiresistive sensor materials correlates with a higher response to gas adsorption on the SMO. However, the vague gas selectivity and low tolerance to moisture, stemming from the surface carrier-concentration-dependent electrical resistance change mechanism, are considered significant drawbacks.

In chemiresistive gas sensors, the response is typically expressed as the ratio of electrical resistance in air (R_{air}) to electrical resistance under target gas (R_{gas}), as R_{air}/R_{gas} or R_{gas}/R_{air}, or as $\Delta R/R_{air}$ or $\Delta G/G_{air}$ (where G represents conductance, the inverse of electrical resistance, R^{-1}) in most reports. One of the important gas sensing performances is the limit of detection (LOD), which is the lowest detectable gas concentration. It is defined as 3 times the noise level of electrical resistance under air ($LOD = 3 \times rms_{noise}/S$). Here, rms_{noise} represents the standard root-mean-square noise of the sensors, and S is the sensitivity (dy/dx, where dy is the change in the sensor's electrical resistance and dx is the change in gas concentration). The response and recovery times, which quantify the sensing speed of the sensors, are generally defined as the time taken to reach 90% of the maximum electrical resistance change under target gas from R_{air}, and the time to return to 10% of R_{gas} from the initial electrical resistance after the target gas exposure is turned off. The response of conductance-based chemiresistive gas sensors (noted as $\Delta G/G_{air}$) is similarly defined, with response and recovery times measured in the same way.

2.2. Capacitive sensor

A capacitive gas sensor is a type of electrical sensor that operates based on changes in capacitance, which are influenced by the dielectric constant and the thickness of the dielectric layer after gas adsorption on a porous SMO surface using alternating current (AC). Unlike electrical resistance-based sensors, capacitance in a capacitive sensor is determined by the equation $C = \varepsilon A/d$, where A is the area of the electrode, d is the separation distance between two electrodes and described as thickness. The important parameter ε is the permittivity

derived by multiplying the vacuum permittivity (ε_0) and relative permittivity (ε_r) described as $\varepsilon = \varepsilon_0 \times \varepsilon_r$. Therefore, the mechanism of a capacitive sensor relies on changes in the dielectric constant of the sensing layer, without involving charge carrier transport through the SMO. Capacitive gas sensing devices typically utilize parallel plate and interdigital electrodes (IDEs) structures. The simplicity of the capacitive sensor's structure offers several advantages, including higher sensitivity, ease of integration into systems with low fabrication costs, practical reliability, and general independence from the electrode material[27−34].

Capacitive gas sensors operate through several mechanisms. First, capacitance changes can be observed from the C-V plot due to variations in depletion layer thickness. Specifically, capacitance can change in two primary ways: through alterations in the work function and charge density. When the target gas is directly adsorbed onto the porous SMO surface or the metal electrode, it becomes polarized, affecting the junction interface between different materials such as metal-MOS (metal-oxide-semiconductor) and MOS-substrate. This leads to changes in charge carriers or dipole polarization, which in turn modifies the depletion layer thickness. This effect is typically reflected in a shift of the flat-band voltage (bias), with the shift increasing depending on the concentration of the target gas. Secondly, the different resonant frequencies (f) of each gas molecule, which are associated with their respective inherited relative permittivity (ε_r), can be used for gas detection. The relationship between resonant frequency and permittivity is inversely proportional, as described $f \propto 1/\varepsilon_r^{1/2}$. The resonant frequency indicates the optimized frequency for gas sensing and can help to identify specific gas species within a certain frequency range. Additionally, impedance changes can also be employed for capacitive gas sensing through LCR (inductance-capacitance-resistance) measurements. The Cole-Cole plot (or Nyquist plot) of the equivalent circuit (with Z' as electrical resistance on the x-axis and Z'' as impedance on the y-axis) illustrates the electrical resistance and capacitance corresponding to different frequencies. The distribution of contributions from the bulk, grain boundary, and electrode to resistivity and capacitance changes across variable frequencies offers a detailed insight into the gas sensing mechanism[27−34].

The response, limit of detection (LOD), and response/recovery times of capacitive gas sensors are conceptually similar to those of chemiresistive sensors. The response is expressed as $\Delta C/C_{air}$, where C_{air} is the baseline of capacitance value under air, and ΔC is the difference between capacitance under target gas (C_{gas}) and C_{air}. Response time and recovery times are defined as the time taken to reach 90% of the maximum C_{gas} and the time taken to return to 10% from C_{gas} to C_{air} after gas desorption begins on the SMO surface, respectively. The LOD of the capacitive sensor is calculated as $LOD = 3 \times \sigma/S$, where σ is the standard deviation of capacitance in baseline, and S is the slope of the fitting curve for a response, respectively[35−39].

2.3. Field-effect transistor sensor

Field-effect transistors (FETs) for gas sensing are similar to MOSFETs, consisting of a source, drain, gate electrode, substrate, and SMO for the gas adsorption area. FET devices are generally distinguished by the position of the gate electrode or the type of gate material, such as back-gate, top-gate, dual-gate, floating gate, horizontal floating gate, suspended gate, capacitively coupled gate, and catalytic metal gate, among others. Similar to chemiresistive and capacitive gas sensors, the adsorption of target gases on the SMO surface leads to changes in charge carriers, resulting in altered electrical conductivity[40−51]. This change is measured by the output current (I_{DS}) versus the voltage (V_{DS}) for different applied gate voltages (V_{GS}), or I_{DS} versus V_{GS} for a fixed V_{DS}. These electrical output changes originate from the intrinsic electronic properties of the SMO, such as band gap, work function, carrier mobility, and defect density. The modulated electronic structure of the SMO, influenced by the adsorbed gas molecules, primarily adjusts charge carrier mobility, which is crucial for gas sensing operations. Additionally, the height of the Schottky barrier between the SMO and the metal electrode is critical, not only for proper carrier conduction in an air environment but also for its response after gas exposure. The Schottky barrier height is determined by the band structure mismatch between the materials, and it plays a significant role when gases are adsorbed on the SMO surface. Upon gas adsorption, the Schottky barrier can shift either upward or downward, depending on the type of gas molecule, with larger shifts occurring at higher gas concentrations. Therefore, the FET gas sensing mechanism, along with the various device structures, offers a higher degree of flexibility in device fabrication. Moreover, FET gas sensors demonstrate ease of integration into systems, similar to commercialized chips or device structures, and hold great potential for diverse applications, including flexible, portable, and IoT devices, with reliable sensing performance.

2.4. Mass-sensitive sensor

A mass-sensitive gas sensor, also known as a gravimetric gas sensor, is a type of microelectromechanical system (MEMS) device. When analyte gas molecules adsorb onto the surface of SMO, a small increase in mass occurs, which can be detected by measuring the change in the electric signal. This change is due to a decrease in resonant vibration frequencies, as detected by a piezoelectric device. The primary devices used in mass-sensitive gas sensors vary based on their structural differences, including cantilevers, quartz crystal microbalances (QCMs), surface acoustic wave (SAW) devices (where acoustic waves propagate laterally across the piezoelectric substrate), bulk acoustic wave (BAW) devices (where acoustic waves propagate vertically through the piezoelectric substrate), and film bulk acoustic resonators (FBARs). When an SMO layer is coated onto the piezoelectric crystal substrate, it enhances the

adsorption of target gases, leading to a mass change in the device, which is then immediately converted into an electrical signal due to the oscillation frequency shift[52−60]. The response mechanism of a mass-sensitive gas sensor is defined by the frequency difference between the initial state and after gas adsorption, denoted as Δf (f_{gas} -f_{air}). As the concentration of gas molecules increases, the frequency shift becomes more pronounced, allowing the identification of gas species based on their chemical sensitivity, which is the ratio of frequency shift to gas concentration (Hz/ppm). The limit of detection (LOD) is typically defined as the gas concentration that produces a frequency shift three times greater than the noise level[52−60].

2.5. Optical sensor

Optical gas sensors operate by detecting electromagnetic radiation changes due to permittivity variations in the gas-adsorbed SMO, which affect the propagated resonant frequencies[61−63]. Typically, an optical sensor comprises three basic components: a radiation source, an interaction volume where gas molecules adsorb onto the SMO, and a detector. This review discusses several types of optical gas sensors, including photonic crystal gas sensors, optical fiber sensors, surface plasmon resonance (SPR) sensors, and surface-enhanced Raman scattering (SERS) sensors[31−36]. Photonic crystal gas sensors utilize the diffraction properties of light propagated through dielectric SMO materials. When target gases adsorb onto the SMO surface, the SMO's band structure adjusts, resulting in shifts in the diffracted wavelengths or frequencies. This shift is explained by the combined Bragg's law and Snell's law: $m\lambda = 2d(n_{eff}^2 - \sin\theta^2)^{1/2}$ where m is the order of reflection, λ is wavelength of diffraction light, d is distance between particle planes, n_{eff} is the mean effective refractive index, θ is the angle of diffraction light. When gas molecules diffuse into the porous spaces of photonic crystal materials, the detected wavelength peak shifts are determined by the n_{eff} values of the gases or by changes in the SMO's n_{eff} after gas adsorption. Optical fiber sensors replace the cladding of optical fibers with SMO coatings, creating various designs such as cladding-off multimode fiber, tapered optical fiber, and D-shaped optical fiber. Light propagates through these fibers via internal reflection, according to Snell's law. After analyte gas adsorption, the SMO's n_{eff} changes, modulating the wavelength emitted from the radiation source and increasing the detected intensity in Raman spectroscopy. SERS sensors enhance surface plasmon excitation when target gases adsorb onto suitable materials and nanostructures. To develop ultrasensitive SERS sensors using SMO, numerous studies have focused on structural engineering to fabricate lower-dimensional particle structures, enhance chemical coupling between gas molecules and the SMO surface, and create noble metal-SMO or conductive organic-SMO composites to facilitate charge carrier transfer, taking into account the electronegativity and electronic structure of each species[64−72].

As introduced above, optical sensors measure wavelength changes after gas adsorption onto the SMO surface. The adsorbed analyte gases induce changes in the dielectric constant and electronic structure through carrier transfer, which is detected by the light source. Optical sensors utilize a diverse range of formats based on sensing mechanisms that combine Bragg's law and Snell's law, distinguishing them from other types such as chemiresistive, capacitive, and mass-sensitive sensors. Regarding the gas response determined by specific λ, $\Delta\lambda$, and Δn_{eff} values associated with different gases and their concentrations, optical gas sensors provide superior gas distribution detection due to their specific response at characteristic wavelengths depending on the gas molecules. As a result, optical sensors are conventionally used in industrial settings to monitor hazardous gases in exhaust systems.

In summary, gas sensors can be classified into various types based on their operating principles, including chemiresistive, capacitive, FET, mass-sensitive, and optical sensors. Most gas sensors, such as chemiresistive, capacitive, and FET sensors, rely on detecting electrical differences before and after exposure to target gas molecules, primarily through surface charge density modulation. These sensors offer fast response times, high sensitivity, and compatibility with diverse integrated device formats. However, they often exhibit limited gas selectivity due to their one-way response mechanism. Mass-sensitive sensors, including QCMs and SAW sensors, detect mass changes upon gas adsorption, enabling ultra-sensitive detection with miniaturization potential. However, they face challenges in minimizing environmental noise to ensure precise signal detection. Lastly, optical sensors monitor changes in light λ, n, or intensity upon gas adsorption, allowing for highly accurate gas species identification with excellent selectivity. However, their complex instrumentation makes them more suitable for industrial applications such as hazardous gas monitoring and process control. Each sensor type has unique strengths and trade-offs, and their selection depends on specific requirements for sensitivity, selectivity, response time, and environmental stability in applications such as air quality monitoring, industrial safety, and environmental sensing.

3. A basic concept of MOFs and fabrication techniques of MOF films

3.1. Brief introduction of MOFs

In 1999, MOF-5 was first reported by the Yaghi group and they viewed the oxide-centered cluster as a secondary building unit (SBU) capable of assembly with dicarboxylate. Through X-ray diffraction study, its composition and structure were revealed. The formula in the presence of solvents was $Zn_4O(BDC)_3\cdot(DMF)_8(C_6H_5Cl)$ and that without solvents was $Zn_4O(BDC)_3$. The structure and space group were suggested to be a simple cubic six-connected net and *Fm-3m* as can be seen in Figure 2(a). Due to its isoreticular structure, MOF-5 has been called Isoreticular MOF-1 (IRMOF-1). This MOF displays a type-I reversible N_2 isotherm and a high specific Langmuir surface area of 2 900 $m^2\cdot g^{-1}$[37].

Hong Kong University of Science and Technology-1 (HKUST-1) was first announced in 1999 by Chui group, and

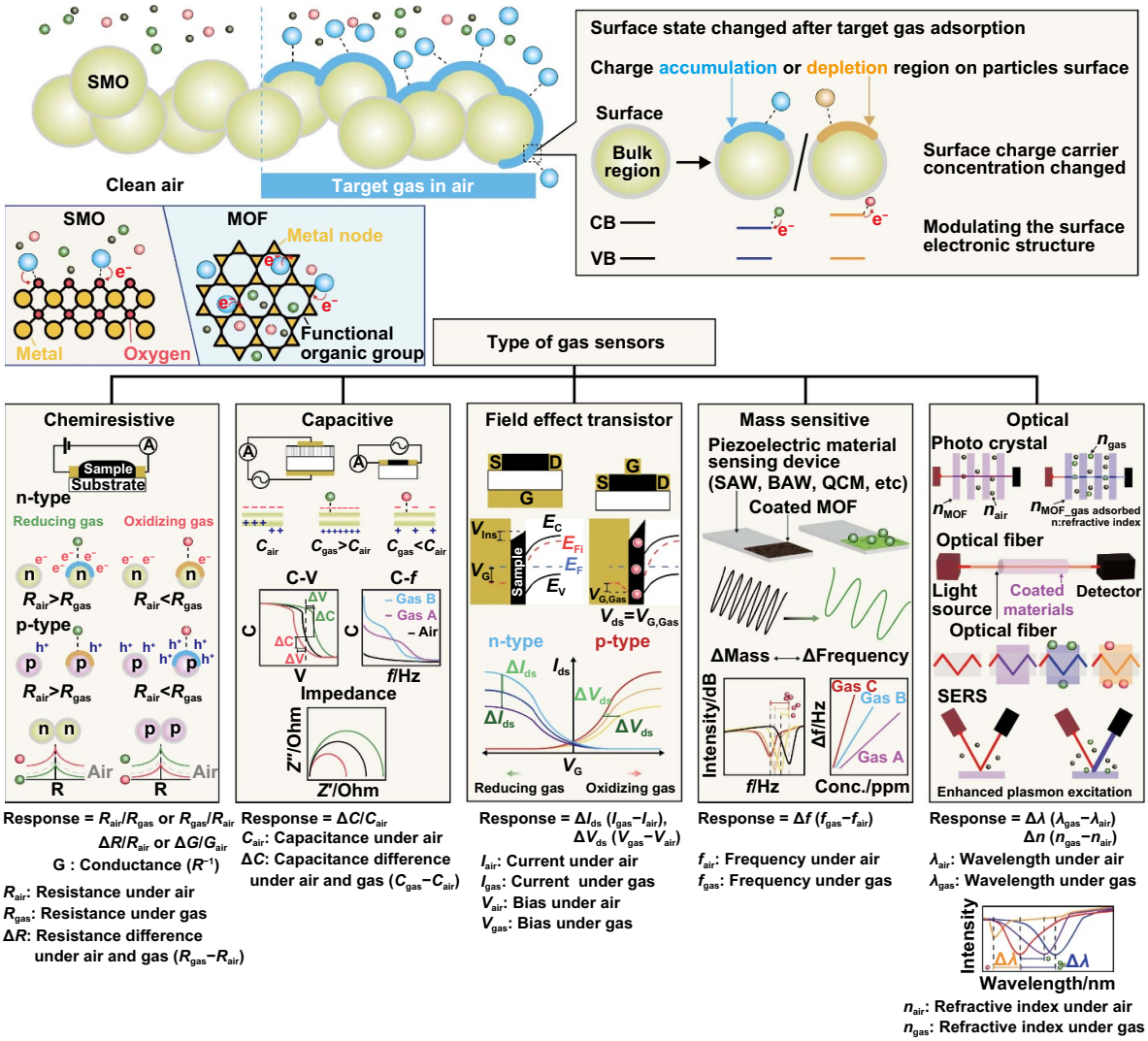

Response = R_{air}/R_{gas} or R_{gas}/R_{air}
$\Delta R/R_{air}$ or $\Delta G/G_{air}$
G : Conductance (R^{-1})
R_{air}: Resistance under air
R_{gas}: Resistance under gas
ΔR: Resistance difference under air and gas ($R_{gas}-R_{air}$)

Response = $\Delta C/C_{air}$
C_{air}: Capacitance under air
ΔC: Capacitance difference under air and gas ($C_{gas}-C_{air}$)

Response = ΔI_{ds} ($I_{gas}-I_{air}$), ΔV_{ds} ($V_{gas}-V_{air}$)
I_{air}: Current under air
I_{gas}: Current under gas
V_{air}: Bias under air
V_{gas}: Bias under gas

Response = Δf ($f_{gas}-f_{air}$)
f_{air}: Frequency under air
f_{gas}: Frequency under gas

Response = $\Delta\lambda$ ($\lambda_{gas}-\lambda_{air}$) Δn ($n_{gas}-n_{air}$)
λ_{air}: Wavelength under air
λ_{gas}: Wavelength under gas
n_{air}: Refractive index under air
n_{gas}: Refractive index under gas

Figure 2. The type of gas sensor and gas sensing mechanism for chemiresistive, capacitive, field effect transistor, mass sensitive, and optical gas sensors.

they adopted solvothermal chemistry to the copper trimesate system. X-ray structure analysis showed that HKUST-1 is composed of dimeric cupric tetracarboxylate, its formula is $Cu_3(TMA)_2(H_2O)_3$, and the space group corresponds *Fm-3m*. It has 1 nm-sized nanochannels with a size of 9.5 Å × 13.3 Å along [100] direction and hexagonal-shaped windows with a size of 18 Å along [111] direction (Figure 2(b)). To evaluate its porosity, N_2 isotherm was obtained and the specific surface area was calculated to be 692 $m^2 \cdot g^{-1}$ (Brunauer–Emmett–Teller, BET) and 918 $m^2 \cdot g^{-1}$ (Langmuir)[38].

Chromium was one of the challenging elements to be incorporated into MOFs, and to this end, Matériaux de l′Institut Lavoisier-53 (MIL-53) was developed and first presented in 2002. By investigating the X-ray pattern, the formula of Cr(III)OH(BDC) was confirmed (Figure 2(c)), and it was found that the Cr polyhedral shares the μ_2 hydroxyl group forming a linear chain. The N_2 isotherm at 77 K was obtained and the specific Langmuir surface area was calculated to be 1 500 $m^2 \cdot g^{-1}$[39].

Universitetet I Oslo-66 (UiO-66) is notable in that it is based on zirconium oxide, and it was first reported in 2008. The formula and space group were $Zr_{24}O_{120}C_{192}H_{96}$ and Fm-3m. Zr_6-octahedron are alternatively capped by μ_3-O and μ_3-OH groups, and by connecting dicarboxylate, $Zr_6O_4(OH)_4(CO_2)_{12}$ came out. The 12 coordination of metal atoms indicates a closed-packed structure, leading to the crystal in a cubic close-packed structure as can be seen in Figure 2(d). The specific Langmuir surface area of 1 187 $m^2 \cdot g^{-1}$ was derived from N_2 isotherm at 77 K[40].

As noticed from the name, the assembly way of ZIF-8 is similar to that of aluminosilicate zeolite consisting of Si or Al connected by O, and instead, ZIF-8 is built from Zn ions connected by 2-methylimidazolate (2-MeIM) linker[41,42]. X-ray diffraction analysis showed that the space group is I-43 m and Zn ion is tetrahedrally coordinated by 4 nitrogen atoms and capped by imidazolates, as can be seen in Figure 2(e). Additionally, the effective diameter of cages was 12.5 Å and the effective window size was 3.3 Å. The framework

decomposition was found in the range of 400 °C to 550 °C and the specific Langmuir surface area was 1 400 $m^2 \cdot g^{-1}$.

One of the prototypical MOFs with open metal sites is M-MOF-74, and Zn-MOF-74, or CPO-27-Zn was first reported in 2005. Mg-MOF-74, one of the analogues with lightweight divalent metal ions, was first reported in 2008, and the yellow crystalline material was obtained through solvothermal reactions of $Mg(NO_3)_2 \cdot 6H_2O$ and DOBDC in DMF/ethanol/water. By investigating powder X-ray patterns, it was found to be isostructure with those of MOF-74 series, as can be seen in Figure 2(f). The unit cell was a trigonal cell (a: 26.0 Å, c: 6.72 Å) and the specific surface areas of 1 905 $m^2 \cdot g^{-1}$ and 1 495 $m^2 \cdot g^{-1}$ were derived from N_2 isotherm at 77 K[43].

3.2. Electrical properties of MOFs: from insulator to electrical conducting material

While the crystalline structure and the properties of MOFs are important for gas sensors. Its electrical properties are fundamentally critical to determining the structure of the sensor and sensing mechanism[3,21,44]. Therefore, we briefly summarize the factors affecting the electrical properties of MOFs. As we explained in the introduction, most MOFs are insulators due to their structural composition and the nature of the materials used. MOFs consist of metal ions or clusters connected by organic linkers through coordination bonds. A major factor contributing to their insulating nature is the use of organic linkers, which are often non-conductive[45]. For example, common linkers, such as carboxylates or phosphonates, do not have extended π-conjugation, which is necessary for facilitating electron transport. As a result, the electrons remain confined to specific atoms or bonds, leading to insulating behavior. Furthermore, many MOFs have large electronic band gaps, meaning the energy required to move electrons from the valence band to the conduction band is high, indicating that electron excitation is low under normal conditions. In addition, while the amounts of metals are not negligible, metal atoms are separated by the organic linkers, not allowing electron transport through the metal clusters.

Recently, many results have been reported regarding electrically conductive MOFs. Considering the reasons for the insulating properties, electrically conductive properties can be achieved by the combination of a proper metal and organic linker. The history of conductive MOFs has been summarized in the literature, but we summarize critical factors[45−48]. Conductivity can arise by incorporating π-conjugated organic linkers, which allow for electron delocalization and create pathways for electron movement between metal centers. In addition, when metals like iron or copper exist in multiple oxidation states, electron hopping between metal ions can be allowed. In other cases, close metal-metal interactions, either through proximity or conductive linkers, facilitate electron transfer. Additionally, guest molecule doping can enhance conductivity by introducing charge carriers (electrons or holes), which help electrons move more easily through the framework. Furthermore, MOFs with 2-D layered structures often show improved conductivity due to the efficient pathways for electron transport created by the closely packed metal centers within the layers. A good example of conductive MOF is $Cu_3(HHTP)_2$, where Cu stands for copper and HHTP stands for hexahydroxytriphenylene. In the MOF, highly electrically conductive properties have been reported because of the combined effect of conjugated linker systems, mixed metal centers, and 2-D layered structures. While the aforementioned approaches are effectively investigated, they are still challenging, and many rooms remain undiscovered for gas sensor applications.

3.3. Strategies for reforming MOFs to be tailored for gas sensing

3.3.1. Tuning MOFs for facile gas transport and adsorption. Gas sensing is accompanied by gas transport and adsorption, and facile access to active sites and favorable specific gas adsorption ensure high performance in gas sensing regardless of working principles. Various strategies have been reported and verified. Simply, thinning MOF films, decreasing MOF particle size and growing oriented morphologies have been suggested to facilitate accessible gas transport, which can lead to effective variations in electrical resistance, capacitance, work function, mass, refractive index, and resonance units[49]. Also, because each MOF possesses a unique aperture size and can be utilized for separating targeted gas molecules, tunning aperture size by changing metal elements or organic linkers can be effective[50].

Adjusting pore size distributions of MOFs can be a positive solution because pore size also governs the interaction with gas molecules[51]. Additionally, the formation of polar surfaces within MOFs facilitates the capture of diverse polar gases (e.g. H_2O, C_3H_6O, NH_3, O_3, etc.) more favorably with strong electrostatic interaction, enhancing both selectivity and sensitivity[52,53]. Some MOFs can have open metal sites by removing labile molecules, and they play roles in strong gas adsorption sites though too much favorable bonding with gas molecules sometimes destroys the structures[54].

3.3.2. Use of hydrophobic organics and MOFs. Water vapor in the air significantly affects the gas sensing performance due to higher affinity with MOFs than that of other gases and is preferentially adsorbed. From time to time, MOFs undergo decomposition by reacting with water vapor and then, it cannot work properly anymore. Therefore, coating with materials containing long hydrophobic alkyl chains like octadecyltrimethoxysilane on MOF films, incorporating hydrophobic functional groups (e.g. trifluoromethoxy group) into organic linkers, using water-stable MOFs like UiO-66 in gas separation membranes can be effective strategies[55].

3.3.3. Extension of charge transport pathways within MOFs. Highly conductive MOFs are captivating in gas sensing, and the strategies for realizing it can be established based on charge transport pathways such as bonding, extended conjugation, space, and guest molecules[45]. First, MOFs are built

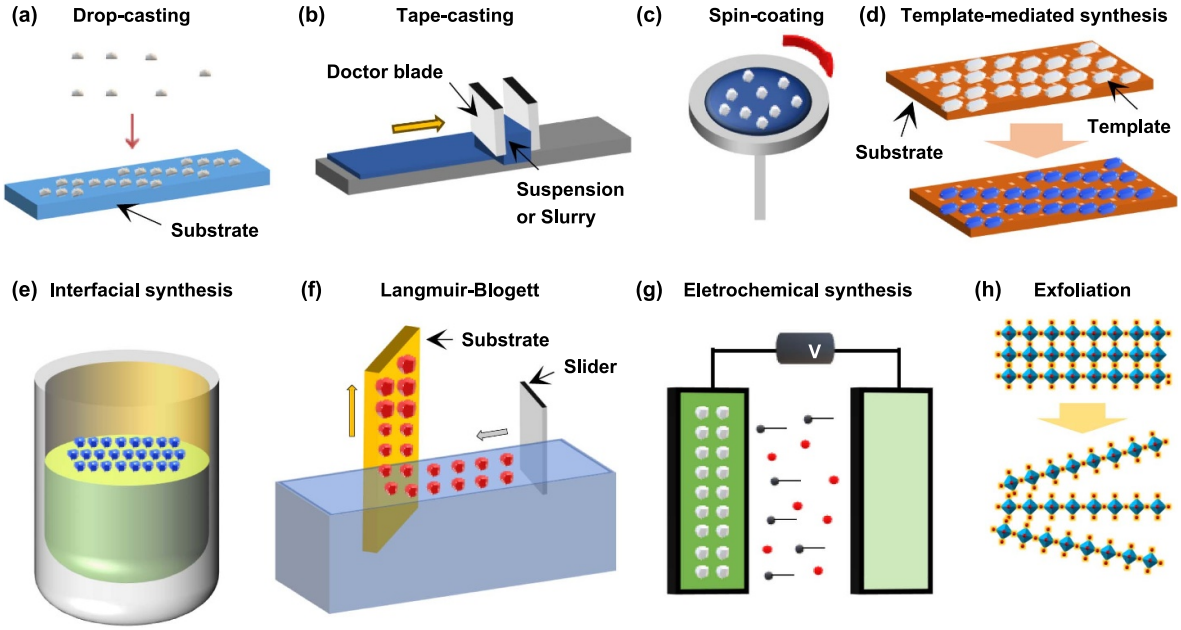

Figure 3. A schematic diagram of various fabrication methods for MOF films. (a) MOF solution dropping onto substrate. (b) MOF suspension or slurry following doctor blade. (c) MOF solution forced by centrifugal force. (d) MOF formation along template. (e) MOF formation between two phases. (f) MOF solution following along substrate. (g) movement of MOF precursors caused by electrochemical reaction. (h) exfoliation of MOF crystals.

from bonding involving the orbital overlap of metals and organic linkers, leading to the construction of a small band gap and becoming one of the critical charge transport pathways. Therefore, finding well-matched combinations of metals and organic linkers for small bandgap and their continuous formation in a consistent direction would give rise to highly conductive MOFs. Secondly, similarly, organic linkers incorporating chelating functional groups that are conjugated with organic cores like 2,3,6,7,10,11-hexaaminotriphenylene can form π-d conjugation, allowing for delocalization of charge carriers and high electrical conductivities. Thirdly, as organic linkers come closer, the π-π interaction is stronger, and this space plays a role in a charge transport pathway. Lastly, charge transport pathways can form by post-synthetically incorporating electroactive guest molecules into pores and the transport can proceed through guest-guest or guest-framework.

3.3.4. Integration with catalysts into pores of MOFs. Exploiting outstanding catalysts and achieving uniform distribution of catalysts is very effective in dramatically enhancing catalytic performance[56]. The regular small pores of MOFs can be great nucleation sites for catalysts showing the previously mentioned properties and stabilizing small catalysts preventing agglomeration. Meanwhile, metal ions in MOFs can sometimes show catalytic activity. The reaction between catalysts and gas species can give rise to reactive elements contributing to performance and variations in the concentration of charge carriers, therefore, the selection of an effective candidate catalyst is critical.

3.4. Various fabrication techniques for MOF films

3.4.1. Drop-casting. Drop-casting involves first preparing MOF solutions and then dropping them onto substrates, and the evaporation of solvent leads to a film consisting of remaining MOFs as seen in Figure 3(a). This is one of the simplest and fastest processes to fabricate MOF films, so most MOF sensors have been fabricated using this method[57]. This method doesn't require specific equipment, and volatile solvents are generally used. However, because several factors determine the final incorporated MOFs, careful adjustment is required. The factors include types, surface functionalization, angles of substrates, surface defects such as cracks and holes, temperature, and humidity. In addition, the coffee ring effect left some patterns after solvent evaporation. Therefore, reproducible production is challenging in industrial fabrication.

3.4.2. Tape-casting. Tape-casting is a well-known casting process for the mass production of ceramic tape and is called doctor blading as well. First, the doctor blade is adjusted at a fixed distance from a substrate, and suspension or slurry containing MOFs is situated in front of the doctor blade. While the doctor blade moves forward along the substrate with constant velocity, followed by a drying process, thin films with constant thickness are fabricated as shown in Figure 3(b). The concentration and viscoelastic properties of suspension or slurry, types of solvents, the distance between the doctor blade and substrate, velocity of the doctor blade, etc., govern features of final MOF films. This method has the advantages of easy control of thickness and being applicable to mass production.

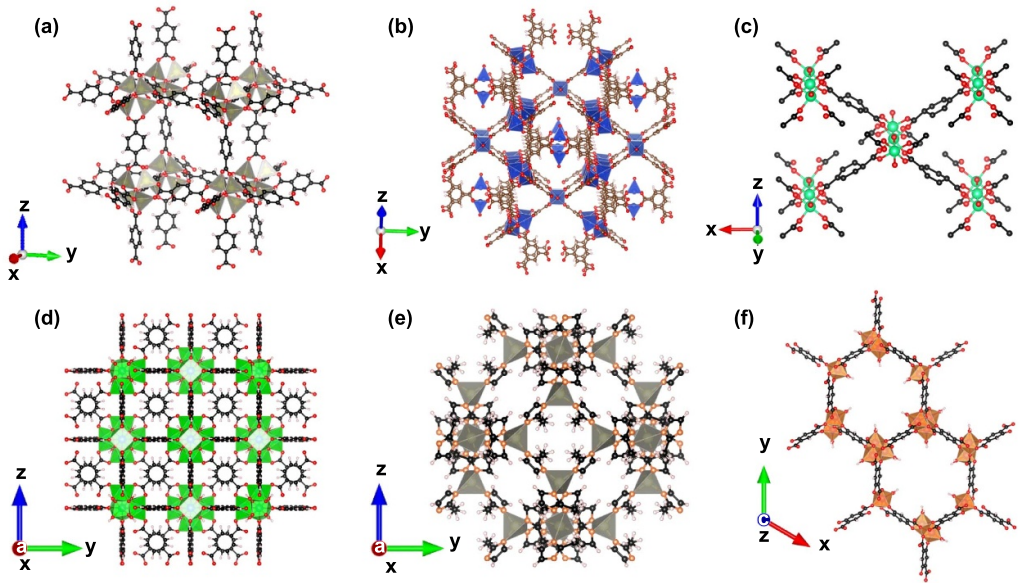

Figure 4. The structures of representative MOFs used for gas sensors. (a) IRMOF-1, (b) HKUST-1, (c) MIL-53(Cr), (d) UiO-66, (e) ZIF-8, (f) Mg-MOF-74. Zn: yellow, C: black, O: red, H: light red, N: orange, Cr: green, Zr: blue, Mg: Pink.

3.4.3. Spin-coating. A substrate is placed on a spin-coater, which is essential equipment for spin-coating. As a spin-coater is rotating, MOF solution is applied on the substrate and the MOFs are then spread by centrifugal force (Figure 3(c)). The solvents are generally volatile and thus, they are evaporated as MOF solution is applied. At higher rotating speeds, thinner films can be fabricated. One of the outstanding advantages is the possibility of realization of uniform thickness. Nonetheless, this method can be used to flat substrates only.

3.4.4. Template-mediated synthesis. Template materials, including metals, metal oxides, and metal hydroxides can provide metal ions during MOF growth without using additional metal sources. By reacting the template materials with organic linkers, MOF growth occurs along the surface of template materials, resulting in thin MOF layers. The scheme of this technique is presented in Figure 3(d), and this method is mass-productive and cost-effective because most MOFs are commonly removed during the sensor fabrication. When the metal source and organic linker source are mixed in solution, the reaction is hard to control and precursors are consumed.

3.4.5. Interfacial synthesis and Langmuir-Blodgett. Interfacial synthesis uses two immiscible solvents that separately dissolve metal ions and organic linkers. When they meet the interface, MOF growth occurs within a very limited space as displayed in Figure 3(e). Depending on interfaces, MOFs displaying various morphologies can be synthesized. Langmuir-Blodgett is named after Irving Langmuir and Katharine B. Blodgett, and the method exploits interfacial synthesis as well. In the beginning, a substrate is soaked into a water reservoir and organic linkers in volatile solvents such as chloroform are spread through the surface of water. Next, the constant surface pressure is applied by performing compression with sliders. The metal salt solution is carefully injected into the water. The MOF growth at the air/water interface is awaited. Then, the substrate and sliders move at constant velocity to collect the MOF nanosheets at the air/water interface (Figure 3(f)).

3.4.6. Electrochemical deposition. Electrochemical deposition can occur at the anode (anodic electrodeposition) or the cathode (cathodic electrodeposition). The metal substrate is used to provide metal ions, which are used to react with organic linkers in electrolyte under electric voltage. During this process, the MOF layer is deposited onto the metal substrate. This technology was first proposed by BASF and has been studied by lots of researchers[58]. Meanwhile, in cathodic electrodeposition, electrochemically generated hydroxide ions from water are deposited on a substrate, deprotonate organic linkers, and deprotonated elements react with metal ions supplied from the electrolyte. This technology was proposed by Dinca group[59]. Generally, the electrochemical method is governed by types of solution composition and substrates, voltage, current density, and deposition time. A brief illustration is presented in the case of anodic electrodeposition (Figure 3(g)).

3.4.7. Exfoliation. The exfoliation method is a top-down process to acquire 2-D MOFs from 3D MOFs as shown in Figure 4(h), and intercalation or sonication of bulk 3-D MOFs can delaminate the layers by interrupting the interaction between the layers. After obtaining a 2-D MOF solution, one can choose one of the previously mentioned deposit methods to fabricate MOF films. A summary of the pros and cons of fabrication techniques is presented in Table 1, and a summary figure of MOFs for gas sensors covered in this paper is presented in Figure 5.

Table 1. A summary of the advantages and disadvantages of fabrication techniques.

Techniques	Advantages	Disadvantages
Drop-casting	Simplicity	Challenging control of thickness, defects, inappropriate for large-scale fabrication, applicable to only planar substrates
Tape-casting	Inexpensiveness, simple, controllable thickness, scalability	Susceptible to various experimental factors
Spin-coating	Controllable thickness	Inappropriate for large-scale fabrication, applicable to only planar substrates
Template-mediated synthesis	Strong adhesion, patternable	Expensiveness
Interfacial synthesis and Langmuir-Blodgett	Finely controllable thickness	Applicable to only planar substrates
Electrochemical deposition	Simplicity, scalability, patternable	Applicable to only conductive substrates, high energy consumption
Exfoliation	Advantage of using surface characteristics	Highly challenging

4. State-of-the-art of MOF-based gas sensors

4.1. MOFs as sensing layers

4.1.1. Chemiresistive MOF sensors. The chemiresistive sensor, which detects electrical resistance changes in the presence of target gases, is the most widely used type of gas sensor due to its simple device structure, low power consumption, reasonable gas sensitivity, and rapid response. As discussed in Section 2, the electrical resistance changes reversibly depending on the gas species and the concentration of adsorbed gases. Increasing the gas adsorption area on the material surface has been a key factor in developing advanced materials. As a result, the high porosity of MOFs has gained attention as a promising candidate for gas-sensing materials. Moreover, MOFs offer additional degrees of freedom in structural design, such as metal clusters, organic linkers, and pore sizes, which can be tailored to achieve larger pores and more active metal sites while maintaining temperature and chemical stability. These unique structural advantages make MOFs a viable option for developing practical chemiresistive gas sensors that are becoming superior to conventional SMO powders. However, the inherent challenges of activating gas adsorption on the surface and the lower electrical conductivity of semiconducting MOFs often necessitate the use of external energy sources or the integration of highly conductive materials to enhance performance[3,21,44,60,61]. In this section, we present examples of improved MOF-based chemiresistive sensors that utilize heating, light sources, and conductive materials to enhance gas sensing performance.

4.1.1.1. Heat-assisted MOF chemiresistive. Lee et al. synthesized Zr–BPDC–SO_2, and Pd@Zr–BPDC–SO_2 samples to use the chemiresistive sensor and show higher sensing performances at 150 °C[62]. These samples, synthesized via a solvothermal reaction, are composed of a 12-connected cuboctahedral $Zr_6O_4(OH)_4(CO_2)_{12}$ cluster and an H_2BPDC–SO_2 sulfone-containing linker in Zr–BPDC–SO_2. The Pd@Zr–BPDC–SO_2 variant involves the metallation of Zr–BPDC–SO_2 with Pd atoms integrated into the framework (Figure 6(a)). To assess gas sensing performance, the sample powders were mixed with α-terpineol to form a slurry, which was then printed onto an electrode-deposited SiO_2 on Si (100) substrate. The gas sensing was measured under 10, 50, and 100 ppm for ethanol, H_2, Benzene, CO_2, Toluene, and HCHO environments between 25 °C and 200 °C. The optimal gas sensing temperature for Zr-BPDC-SO_2 was determined to be 150 °C, based on gas response (R_{gas}/R_{air}), which increased up to 150 °C but decreased at 200 °C under ethanol exposure. The mechanism of ethanol sensing response is related to oxygen ion adsorption at $Zr_6O_4(OH)_4(CO_2)_{12}$ from ethanol decomposition into CH_3CHO and H_2O. The optimal temperature was attributed to insufficient energy for effective gas adsorption at lower temperatures and a higher desorption rate than the adsorption rate at elevated temperatures (Figure 6(b)). Additionally, Zr-BPDC-SO_2 exhibited a higher ethanol response (between 1.2-1.4 R_{gas}/R_{air}) compared to a lower response (1.1 R_{gas}/R_{air}) for other gases, with a proportional relationship to target gas concentration. Meanwhile, the Pd@Zr-BPDC-SO_2 sample showed a significantly higher gas response (over 1.9 R_{gas}/R_{air}) to H_2 gas at 100 ppm compared to a lower response (1.3 R_{gas}/R_{air}) for other gases, due to the enhanced catalytic effect between Pd and H_2 molecules, which activated adsorption sites for hydrogen gas in Zr-BPDC-SO_2. This study highlights the importance of heating gas-sensing materials to the appropriate temperature that modulates the balance between adsorption and desorption.

4.1.1.2. Light-assisted MOF chemiresistive. Jo et al. proposed an alternative method for providing external energy during gas sensing through light activation, utilizing photocatalytic mechanisms to enhance adsorption reactions and desorption processes, thereby enabling faster recovery of the material's surface. The visible light on $Cu_3(HHTP)_2$ (HHTP = 2,3,6,7,10,11-hexahydroxytriphenylene) nanoflakes and Fe_2O_3 activated

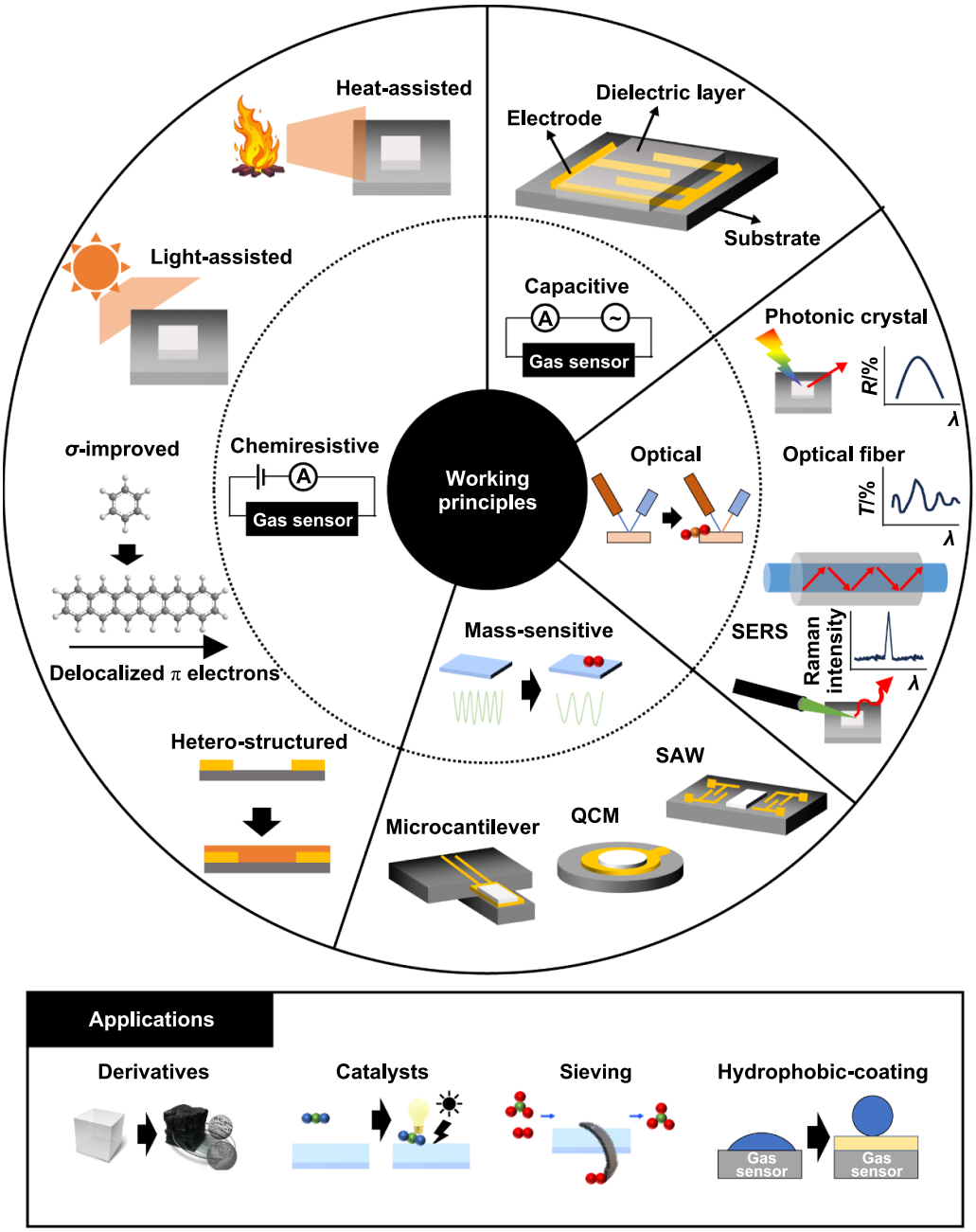

Figure 5. A summary figure of MOFs for gas sensors.

the desorption of NO_2 gas[63]. $Cu_3(HHTP)_2$ nanoflakes were synthesized via a solvothermal reaction, followed by two centrifugation steps to produce $Cu_3(HHTP)_2$-NFs. Subsequently, Fe_2O_3 nanopowder slurry was mixed with the $Cu_3(HHTP)_2$-NFs slurry to achieve a 2:1 weight ratio of $Cu_3(HHTP)_2$-NFs to Fe_e2O_3 nanopowder, forming a hybrid structure. The sampling process involved drop-casting the $Cu_3(HHTP)_2$-NFs and Fe_2O_3 slurry onto a patterned SnO_2 electrode on a transparent PET substrate, followed by solvent removal at 60 °C for 30 minutes. Gas sensing was performed at room temperature using 5 ppm of various analyte gases, including NO_2, HCHO, C_6H_6, CO, C_3H_6O, H_2, C_2H_5OH, p-xylene, toluene, and NH_3. The $Cu_3(HHTP)_2$ nanoflakes exhibited an 89.4% response to NO_2, compared to 61.1% for coarser $Cu_3(HHTP)_2$ flakes, indicating a greater abundance of gas adsorption sites on the $Cu_3(HHTP)_2$ surface for NO_2, with negligible reactions to other gases. The issue of irreversible NO_2 gas adsorption was addressed through visible light exposure, which facilitated the desorption of NO_2 from $Cu_3(HHTP)_2$ flakes. Greater desorption was observed under blue light (2.76 eV), which has higher energy than lower-energy bright light. Furthermore, the Fe_2O_3 nanopowder and $Cu_3(HHTP)_2$-NFs exhibited full recovery to Rair under blue light exposure, as the heterojunction between Fe_2O_3 and $Cu_3(HHTP)_2$-NFs promoted the desorption of adsorbed NO_2 by generating more photoinduced holes and extending their lifetime. This study demonstrated

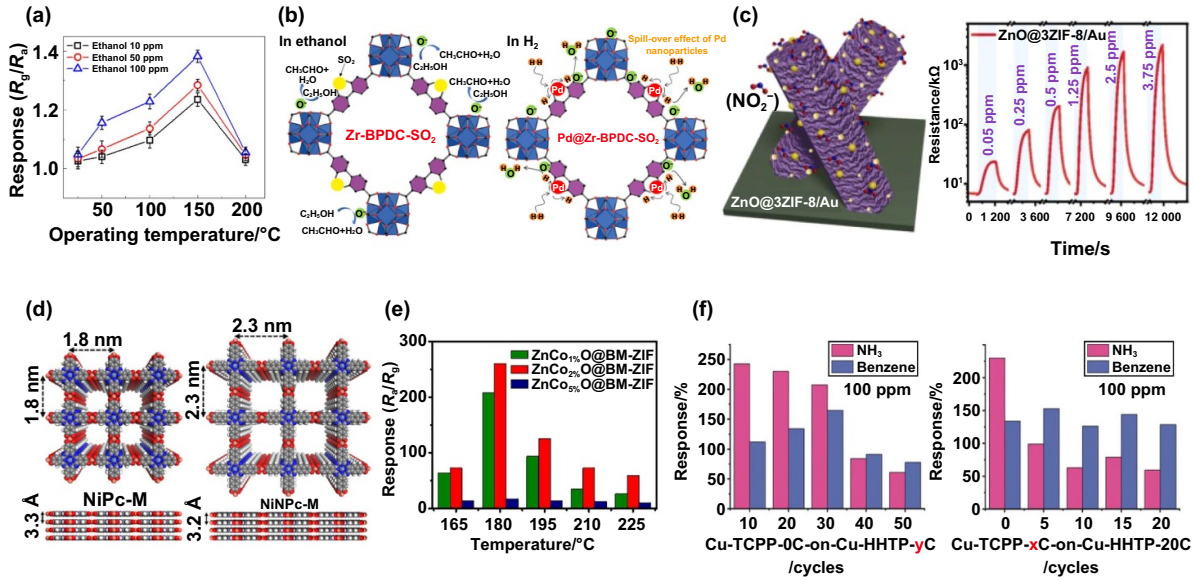

Figure 6. Chemiresistive MOF sensor. (a) Temperature dependence gas sensing performance under ethanol on Zr-BPDC-SO_2 to explain the sensing dynamic response of MOF sensor at 150 °C. (b) The structure of Zr-BPDC-SO_2 and Pd@Zr-BPDC-SO_2 with sensing mechanism. Reprinted from[62], Copyright (2021), with permission from Elsevier. (c) Structure of ZnO@3ZIF-8/Au core-shell heterostructure nanorods and NO_2 sensitivity under UV light. Reprinted from[64], Copyright (2024), with permission from Elsevier. (d) Synthetic scheme for isoreticular phthalocyanine and naphthalocyanine-based MOFs NiPc-M and NiNPc-M. Reprinted with permission from[66]. Copyright (2019) American Chemical Society. (e) The higher H_2S sensing performance in $ZnCo_{2\%}O$@BM-ZIF sensor than the other ratios of ZnCo composition in ZIF structure. Reprinted from[67], Copyright (2022), with permission from Elsevier. (f) The different gas selectivity between MOF-on-MOF thin films such as Cu-TCPP-0C-on-Cu-HHTP-yC and the Cu-TCPP-xC-on-Cu-HHTP-20C for detecting the NH_3 and benzene.[68] John Wiley & Sons. © 2019 Wiley-VCH Verlag GmbH & Co. KGaA, Weinheim.

the enhanced gas sensing performance achieved through photoactivation of the MOF-oxide hybrid, offering a practical approach to gas sensor design that leverages external photon energy for low-temperature operation without the need for heating.

Ling et al. reported the UV-activated NO_2 gas sensing response using Au nanoparticle decorated ZnO@ZIF-8 core-shell heterostructure nanorods at room temperature (Figure 6(c))[64]. The ZnO@ZIF-8/Au is fabricated in 3 steps. First, the growth of ZnO nanorods was performed using a hydrothermal method on a Si substrate. Second, the solution dissolved 2-methylimidazole in 10 ml methanol was spin-coated on ZnO nanorods/Si substrate, and heat treated under 160 °C for 20 min to synthesize ZnO@ZIF-8 core-shell nanorods. The last step was Au decoration using $HAuCl_4$ solution and UV light irradiation on ZnO@3ZIF-8 core-shell nanorods. The gas sensing was measured under 365 nm UV light, and the ZnO@3ZIF-8/Au sensor exhibited higher responses of 260% and 34 700% toward 0.05 and 3.75 ppm of NO_2 environment than the other gases. Under UV light, photogenerated holes supported the desorption of NO_2 gases from the surface, thereby restoring the material's sensing ability. Thus, the UV light activated reversible electronic sensitization through the heterojunctions interface between ZnO@ZIF-8/Au nanoparticles (Each of the elements plays distinct roles: as a gas adsorption site in ZnO, a charge transport channel in 3ZIF-8, and an electron sink with gas adsorption capability in Au), which modulated the depletion region via adsorption/desorption of the NO_2 gases on the ZnO@3ZIF-8/Au surface and measured the highest sensitivity.

4.1.1.3. Electrical conductivity improved MOF chemiresistive. Campbell et al. used conductive MOFs for the chemiresistive gas sensing materials, which measured different electrical conductivities: 0.002 $S \cdot cm^{-1}$ of $Cu_3(HHTP)_2$, 0.2 $S \cdot cm^{-1}$ $Cu_3(HITP)_2$, and 2 $S \cdot cm^{-1}$ $Ni_3(HITP)_2$ to solve the lack of MOF conductivity[65]. The MOF materials were synthesized by solvothermal reaction, and fabrication of the MOF sensor devices was drop-casted using acetone solution and synthesized samples onto interdigitated gold electrodes on a corundum substrate. In addition, the gas sensing array was fabricated by drawing MOF chemiresistors onto paper substrates. The gas-sensing was performed by measuring the electronic conductance when exposured for 30 seconds under 200 ppm concentration of diverse VOC gases such as Haxane, Cyclohexane, Heptane, MeOH, EtOH, *i*-PrOH, Acetone, MEK, THF, Dioxane, Benzene, Toluene, *p*-Xylene, $BuNH_2$, i-Pr_2NH, and ET_3N. The $Ni_3(HITP)_2$ measured a direction of response opposite to Cu-based MOFs ($Cu_3(HHTP)_2$ and $Cu_3(HITP)_2$), which showed a significantly different response from each other. All samples showed responsiveness to VOCs with polar character VOCs but no appreciable response to aliphatic hydrocarbons. The distinct variations in the chemiresistive response of all samples were to distinguish different types of VOCs. This report suggested a charge transfer mechanism for sensing as the d-electron count of the

metal center that induced a pronounced effect on the electronic structure of the MOF and implied electronic interactions with polar analytes. The different gas selectivity for $Cu_3(HHTP)_2$, $Cu_3(HITP)_2$, and $Ni_3(HITP)_2$ was speculated by both strong H-bonding and strongly reducing reactions via metal atoms. Therefore, the different charge transfer and the following hydrogen bonding difference contributed to sensing response and selectivity.

Meng et al. successfully activated chemiresistive gas sensing using bimetallic conductive 2-D MOFs based on metallophthalocyanines (MPCs), specifically NiPc-Ni, NiPc-Cu, NiNPc-Ni, and NiNPc-Cu, synthesized through a solvothermal reaction in Figure 6(d)[66]. The structures of NiPc-M and NiNPc-M were calculated to have pore sizes of approximately 1.8 nm and 2.3 nm, respectively. The MPC samples in this study demonstrated intrinsic conductivity of 10^{-2} $S{\cdot}cm^{-1}$, enabling the use of gas sensors without conductive binders at low driving voltages (0.01–1.0 V). Isoreticular analogs of metallophthalocyanines and metallonaphthalocyanines were shown to modulate gas sensitivity and selectivity to NH_3, NO, and H_2S, with sub-ppm to ppb levels of detection limits (LOD) for NH_3 (0.31–0.33 ppm), H_2S (19–32 ppb), and NO (1.0–1.1 ppb). Principle component analysis revealed that all NiPc-M and NiNPc-M MOFs were capable of distinguishing between NH_3 (40 ppm), H_2S (40 ppm), and NO (1 ppm). This study suggested that the gas sensing mechanisms arise from surface interactions between the analyte gases and the MPC surface, where charge-transfer or redox reactions occur at the metal sites. Furthermore, gas selectivity and sensitivity were influenced by both the inorganic linkers and the π-system in the MPC structure.

4.1.1.4. Heterostructured MOF chemiresistive. Zhou et al. reported a remarkable 130-fold increase in H_2S gas sensing performance using a molecular-sieving MOF membrane on $ZnCo_{2\%}O$@BM-ZIF, as shown in Figure 6(e)[67]. The 3DOM $ZnCo_xO$@BM-ZIF samples were prepared in two steps. First, a macroporous $ZnCo_xO$ substrate was synthesized by creating a PMMA template composed of ∼550 nm rubber spheres using a self-assembly method. A bimetallic precursor solution containing $Zn(NO_3)_2 \cdot 6H_2O$ and $Co(NO_3)_2 \cdot 6H_2O$ (at 0, 1, 2, and 5 wt%) was mixed with citric acid in ethanol and sonicated. This precursor was then infiltrated into the opal templates, dried, and heated at 60 °C for 1–2 hours. The 3DOM bimetallic oxide scaffold was formed by sintering the precursor at 500 °C for 3 hours, removing the PMMA template, and transforming it into $ZnCo_xO$. For the 3DOM $ZnCo_xO$@BM-ZIF samples, the $ZnCo_xO$ substrate was submerged in a 2-MeIM solution and heated at 60 °C for 2 hours to coat the BM-ZIF membrane, followed by washing with ethanol and drying. Among the samples (x = 1%, 5%), the $ZnCo_{2\%}O$@BM-ZIF showed the highest response, with a value of 260, which was 1.3 to 52 times greater than the others. This result was attributed to the proper baseline resistance of 0.93 MΩ for $ZnCo_{2\%}O$@BM-ZIF, compared to 0.9 MΩ for $ZnCo_{1\%}O$@BM-ZIF and 1.01 MΩ for $ZnCo_{3\%}O$@BM-ZIF. The increased resistance was related to the expanded electron depletion layer in the $ZnCo_{2\%}O$@BM-ZIF sensor, which was confirmed by the highest proportion of adsorbed oxygen and the formation of more p-n heterojunctions between n-type ZnO and p-type Co_3O_4 as the Co content increased. The detailed gas sensing mechanism is based on the BM-ZIF membrane, where the interface states of $ZnCo_xO$ were influenced by the organic ligands and the outer film. The synergistic effects of Co and Zn in $ZnCo_{2\%}O$@BM-ZIF significantly enhanced sensing performance through three key mechanisms: (I) molecular sieving by the ZIF membrane, (II) increased catalytic activity of Co sites due to the porous MOF structure, and (III) p-n heterojunctions between ZnO and Co_3O_4. In stage I, the outer BM-ZIF membrane acts as a molecular sieve, allowing smaller gas molecules to pass through more easily than larger ones. BM-ZIF's alkaline sites selectively capture H_2S over other gases. In stage II, Co^{2+} sites enhance the catalytic reaction with H_2S, generating reactive oxygen species. Finally, in stage III, the interaction between ZnO and Co_3O_4 forms a built-in potential barrier, which amplifies resistance changes when exposed to H_2S, significantly improving the sensor's performance.

Yao et al. reported a heterostructured MOF (Cu-HHTP, HHTP = 2,3,6,7,10,11-hexahydrotriphenylene)–MOF (Cu-TCPP, TCPP = 5,10,15,20-tetrakis(4-carboxyphenyl)porphyrin) film used as a highly selective benzene chemiresistive gas sensor operating at room temperature, as depicted in Figure 6(f)[68]. The Cu-TCPP film was synthesized via a solvothermal method and then transferred onto the Cu-HHTP film by a stamping technique. The Cu-HHTP layer itself was prepared by spraying a copper acetate and HHTP solution onto a substrate. The physical integration of different MOF layers with weak van der Waals (vdW) interactions enables a synergistic enhancement of device functionality. While the Cu-HHTP thin film showed a higher response to polar gases like NH_3 at room temperature, the addition of the molecular sieving Cu-TCPP layer on top of the Cu-HHTP layer, combined with vdW forces between the interfaces suppressed NH_3 penetration but developed a higher gas response to benzene at room temperature. This method eliminated the need for lattice matching conditions required by previous techniques for growing MOF-on-MOF heterostructure thin films. Furthermore, this report suggested that integrating a molecular sieving MOF layer onto a chemiresistive sensing MOF layer modulated gas selectivity.

Ghanbarian et al. introduced VOC gas sensing for compounds such as methanol, ethanol, isopropanol, and toluene using a ternary compound conductive MIL-53(Cr-Fe)/Ag/CNT under 10% relative humidity at room temperature[69]. In this study, the bimetallic MIL-53(Cr-Fe) nanostructure was synthesized via a sonochemical method, with Ag nanoparticles and CNTs added to form the ternary composition. The VOC sensing mechanism was related to the structure of the MIL-53(Cr-Fe)/Ag/CNT. The sensor exhibited increasing resistance in response to polar VOCs, with LOD of 30.5 ppm for methanol, 39.6 ppm for ethanol, and 50.5 ppm for isopropanol, while showing decreasing resistance under

exposure to the non-polar gas toluene. The flexible structure of MIL-53(Cr-Fe) provided intercrystalline channels that facilitated the passage of organic vapors, while CNTs acted as conductive fillers, enhancing the performance of the gas sensor. As a result, the resistance of the composite decreased due to the inclusion of CNTs, which provided an electron transport pathway, improving the highly insulating properties of MIL-53(Cr-Fe). Ag nanoparticles further enhanced electron transport throughout the MOF structure and adsorbed oxygen gases. When exposed to reducing polar gases (methanol, ethanol, and isopropanol), these gases captured electrons from the nanocomposite, reducing the material's electrical conductivity. In contrast, when exposed to non-polar gases like toluene, the adsorbed electrons from oxygen returned to the MIL-53(Cr-Fe) film, leading to a reduction in the potential barrier height. Electrons are then transported via the CNTs, increasing conductivity.

4.1.2. Capacitive MOF sensors. As previously discussed, capacitive sensors detect various gases by measuring changes in the dielectric constant or the thickness of the dielectric layer after gas molecules are absorbed[70]. Among various sensor types, capacitive sensors stand out due to their superior stability, ease of manufacturing, accuracy, selectivity, and potential for miniaturization. MOFs are particularly promising as dielectric layers in capacitive sensors because they offer highly ordered structures, large surface-to-volume ratios, and exceptional porosity along with precise control over gas affinity using tunability of active sites and organic ligands. These unique properties facilitate specific surface reactions and the adsorption of target gas molecules, leading to sensitive capacitance variations[71]. As described in Figure 7(a), the capacitive gas sensor measures the capacitance difference before and after adsorption the gas molecules on the MOF surface by modulating surface carrier density. Over the past decades, a variety of MOF-based capacitive sensor systems and designs incorporating different sensing transducer platforms have been proposed. This diversity has driven the development of high-performance capacitive gas sensors for detecting gases such as acetone, ethanol, benzene, CO_2, and SO_2.

Fernandez et al. utilized 1-ethyl-3-methy-Iimidazolium bis(trifluoromethylsulfonyl)imide (([Emim] $[NTf]_2$)) ionic liquid (IL) and Universitetet I Oslo (UiO)-66-$(OH)_2$) MOF to fabricate thin-film capacitive sensors for VOC detection (Figure 7(a))[72]. To facilitate effective integration into electronic circuits, UiO-66-$(OH)_2$ was synthesized via solvothermal methods and then spray-coated with the IL. The electrical response of the fabricated IL/UiO-66-$(OH)_2$ sensor was dependent on the acid dissociation constant (pKa) of the gas molecules. As shown in Figure 7(b), after removing humidity and residual gases from the MOF by heating at 100 °C, the MOF-based capacitive sensor exhibited a linear response to varying concentrations of acetone. Specifically, the IL/MOF sensor demonstrated a sensitivity of 32 $fF{\cdot}sccm^{-1}$ toward acetone. Moreover, it exhibited a response time (τ_{90}) and recovery time (τ_{10}) of less than 1 second, achieving a steady response value thereafter. The sensor showed a distinctive linear relationship between capacitance response and the exponential of gas concentration, correlating with each gas's pKa value (Figure 7(c)). This indicates that the IL/MOF capacitance change varies depending on the gas's acidity, providing selectivity and offering a rational approach to developing highly selective capacitive sensors, given the numerous possible combinations of ILs and MOFs. The intrinsically porous and chemically tunable structures of MOFs provide space for IL incorporation, enabling high ionic conductivity and facilitating sensitive capacitance changes in response to gases with varying pKa values. This may be attributed to the role of MOFs as active components in the electrical response, where their hydroxyl-decorated pore surfaces induce ionic and proton migration within the porous system. Similarly, Chernikova et al. proposed Manchester framework material (MFM)-300 as a sensing layer for a capacitive SO_2 sensor[73]. MFM(In)-300 has a high SO_2 sorption capacity of 8.28 $mmol{\cdot}g^{-2}$ at 25 °C and 1 bar, and it can be fabricated through mild solvothermal methods that ensure circuit stability[74]. The permittivity of MFM(In)-300 changed significantly upon SO_2 adsorption, showing a linear response ranging from 75 to 1 000 ppb and a detection limit as low as 5 ppb. The selectivity toward SO_2 is maintained by both analyte-MOF interactions and analyte-analyte interactions, where adsorbed SO_2 interacts with other SO_2 molecules through dipole interactions on the free bridging hydroxyl group within the pore of MFM-300(In). This results in more than four times higher cross-selectivity against CO_2 and more than twenty times higher selectivity compared to CH_4, H_2, NO_2, C_3H_8, and C_7H_8. Furthermore, the sensor maintained a stable relative capacitance change response over 25 days and during continuous exposure to SO_2.

To enhance the capacitive response of sensors, various on-chip MOF fabrication methods for better circuit integration have been proposed. For example, Xia et al. introduced a one-step solvothermal method to embed Hong Kong University of Science and Technology (HKUST)-1 single crystals on surface-embedded electrodes for ethanol sensing[75]. This method leverages the confined growth of HKUST-1 single crystals around prefabricated metal patterns with varying adhesion strengths. By embedding the electrodes within the MOF, the low base capacitance value was ensured by preventing parasitic contributions from the substrate to the measured capacitance. As a result, at 100 kHz and 0.5 V, the sensor could detect ethanol gas as low as 0.6 ppm, with the relative capacitance response matching the ethanol adsorption on HKUST-1. Additionally, the sensor exhibited distinct capacitance changes at varying ethanol concentrations and demonstrated excellent stability over 225 hours of continuous ethanol sensing at room temperature. This superior performance is attributed to the change in the coordination state of the Cu^{2+} sites in the MOF, which causes capacitance changes upon ethanol exposure[76]. Similarly, Yuan et al. suggested on-chip in situ growth of homogeneous Mg-MOF-74 films via solvothermal methods for benzene and CO_2 detection[77]. The Mg-MOF-74-based capacitive sensor exhibited a positive linear response toward 2 to 100 ppm of benzene and a slightly lower

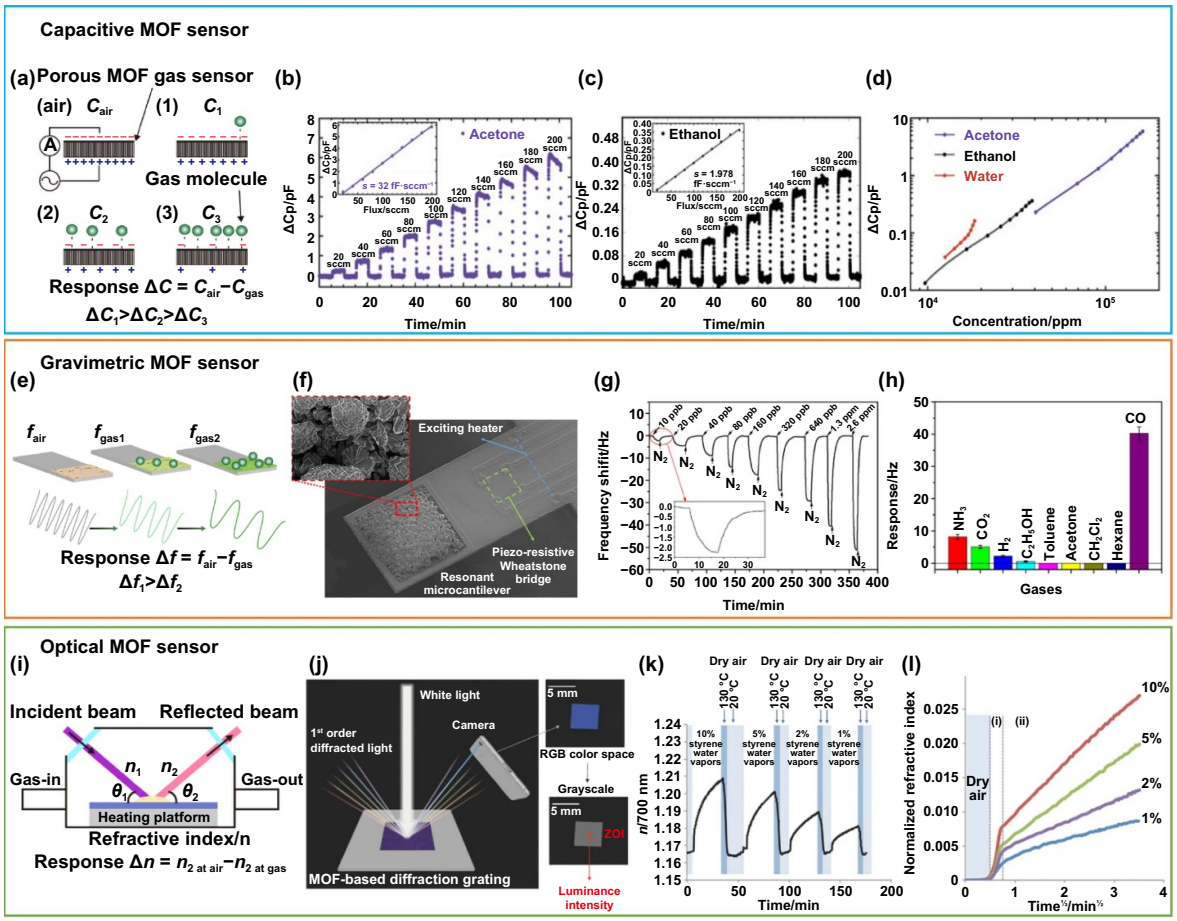

Figure 7. Other types of MOF sensor. (a) Mechanism of capacitive MOF gas sensor. (b) Sensing dynamic of IL/UiO-66-(OH)2 capacitive sensor against various flow rates of acetone, (c) ethanol. (d) Capacitance change of IL/UiO-66-$(OH)_2$ as function of gas concentration (ppm) in the vapor.[72] John Wiley & Sons. © 2021 Wiley-VCH GmbH. (e) Mechanism of gravimetric MOF gas sensor using QCM. (f) Image of gravimetric Ni-MOF-74 loaded microcantilever sensor. (g) Sensing dynamics of Ni-MOF-74 microcantilever sensors against CO gas ranging from 10 ppb to 2.6 ppm. (h) Response of Ni-MOF-74 loaded microcantilever sensor to various interfering gas (1 ppm for all gases).[80] John Wiley & Sons. © 2015 WILEY-VCH Verlag GmbH & Co. KGaA, Weinheim(i) Schematically illustrated optical MOF gas sensor using different n values before and after exposure gas molecules. (j) Illustration of the ZIF-8 photonic crystal based optical sensor. (k) RI variance of ZIF-8 optical sensor against styrene/water vapor ranging 1% to 10%. (l) Plot of the normalized RI as a function of the square root of the time for various vapor concentrations of styrene/water vapor. Reprinted from[81], Copyright (2018), with permission from Elsevier.

positive response toward 200 to 5 000 ppm of CO_2, despite the similar dielectric constants of these two gases.

Furthermore, Mg-MOF-74 did not respond to 5 000 ppm of methane, indicating that the capacitance change likely arises from the MOF's unique chemical tunability and its gas interaction. Specifically, the interaction initiated by π-complexation between the open metal sites of Mg-MOF-74 and the π-electron-rich benzene molecules leads to a significant alteration in the permittivity of the Mg-MOF-74 framework, enhancing its sensitivity to benzene[78]. Furthermore, this study proposed altering the selectivity and sensitivity by reducing porosity and blocking metal sites through postsynthetic functionalization with ethylenediamine, thereby changing the sensor's selectivity. As a result, the sensor's response to benzene was drastically reduced by approximately 60%, while its response to CO_2 was enhanced by approximately 25%. Conversely, the increased basicity from amine groups on the metal sites could adsorb more CO_2 molecules, enhancing sensitivity toward CO_2[79].

Capacitive sensors leveraging MOFs have shown exceptional promise in gas detection due to their precise tunability, high surface area, and superior porosity. Various gases, including VOCs and acidic gases, have demonstrated selective, sensitive, and rapid sensing responses. The unique properties of MOFs, combined with various fabrication processes, highlight their potential for developing high-performance capacitors, paving the way for future applications in a wide array of gas sensing technologies.

4.1.3. Mass-sensitive MOF sensors. Gravimetric sensors operate by using a sensing layer as electromechanical oscillators, detecting gases through changes in resonant frequency caused by mass variations on the surface from

gas interactions[82]. MOF, known for their highly ordered and porous structures, can significantly enhance the sensitivity of gravimetric sensors as they can provide numerous adsorption sites and specific interaction with the gas analyte. Additionally, the selective adsorption capabilities provided by the extensive metal and organic ligand libraries of MOFs contribute to superior selectivity. However, the fabrication process of these sensors requires a strong mechanical coupling and stable bonding with the substrate to ensure precise measurement of frequency changes resulting solely from gas interactions. Consequently, various MOF-based gravimetric sensors with excellent mechanical coupling have been developed, including microcantilevers, quartz crystal microbalance (QCM) sensors, microresonators, and surface acoustic wave (SAW) sensors.

Lv et al. utilized Ni-MOF-74 crystals in resonant microcantilever sensors to detect CO at ppb levels (Figure 7(d))[74]. Ni-MOF-74 sensors were fabricated using solvothermal methods and applied to microcantilevers (Schematically described sensing mechanism in Figure 7(e). The gas response of gravimetric MOF gas sensor using microcantilever is determined by the frequency difference when the gas adsorbed on the MOF mass is changed depending on the gas molecule species and density) through ink printing levels (Figure 7(f)). Among various active metal site candidates, Ni-MOF-74 demonstrated the most favorable adsorption enthalpy (-52.7 kJ·mol^{-1}) toward CO, resulting in the highest sensitivity[83]. The synergetic effect of Ni^{2+} yields specific adsorption interaction with CO and the porous, high surface area of MOF-74 results in numerous adsorption sites for MOF-CO interaction. As a result, it showed a linear frequency shift in the range of 10 ppb to 2.6 ppm CO (Figure 7(g)). Notably, even at 40 ppb CO adsorption, only 16% of the adsorption sites were utilized, indicating the sensor's applicability to higher concentrations. The selectivity of the Ni-MOF-74 microcantilever sensor was also evaluated, showing at least 4.9 times higher response to 1 ppm of CO than to 1 ppm of NH_3, CO_2, H_2, C_2H_5OH, toluene, acetone, CH_2Cl_2, and hexane (Figure 7(h)). Additionally, the sensor exhibited very stable operation with a 1% relative standard deviation response and maintained its performance over six months, with only a 10.5% sensitivity degradation. Furthermore, Cai et al. employed UiO-66 as a sensing layer on a microcantilever to detect dimethyl methylphosphonate (DMMP) at ppb levels[84]. To avoid damage from corrosive precursors and polar solvents during MOF growth on a microcantilever beam, Parylene-C was used as a protective layer for solvothermal growth of UiO-66 on the beam. The UiO-66-loaded microcantilever demonstrated a highly sensitive response to DMMP, with a wide detection range from 5 ppb to 440 ppb and a noise level of less than 0.01 Hz. It also exhibited superior selectivity against various VOCs and showed excellent repeatability, with a difference of only 0.2 Hz between three exposures toward DMMP. This superior gravimetric sensing performance toward DMMP is attributed to the Lewis acidic sites of Zr_6 in UiO-66 over MOF structures, which induce strong adsorption between DMMP and UiO-66, resulting in larger mass changes[85].

As an alternative to microcantilevers, QCM can also be effectively utilized when MOFs are incorporated into the system. Tchalala et al. spin-coated King Abdullah University of Science and Technology (KAUST)-7 and KAUST-8 MOFs onto a QCM electrode to selectively detect SO_2 under atmospheric conditions[86]. KAUST-7 and KAUST-8 exhibit CO_2 and H_2S sieving properties, allowing the KAUST-QCM sensor to selectively and sensitively detect SO_2 in a range of 0 to 500 ppm under a nitrogen environment. In atmospheric environments with humidity and interfering gases, the sensitivity was slightly reduced, but the sensor still responded sensitively to 25–500 ppm of SO_2. It also demonstrated four times higher sensitivity toward SO_2 compared to other gases and maintained its sensitivity for 12 days. Similarly, Zhang et al. utilized ZIF-90-based QCM sensors for superior detection of acetone[87]. ZIF-90 was synthesized via solution methods and applied to the QCM sensor through drop casting. Acetone interacts strongly with the aldehyde group of ZIF-90, resulting in a rational adsorption enthalpy. Consequently, the ZIF-90-based QCM sensor showed high sensitivity of 95 Hz toward 1 ppm acetone, with a detection limit of 20 ppb. Furthermore, its adequate adsorption enthalpy enabled a fully reversible and stable response, with response and recovery times of 12 seconds and 17 seconds, respectively, and maintained performance over 70 days. The special interaction between ZIF-90 and acetone results in selective detection of acetone among other VOCs, including CH_2O, C_2H_5OH, NH_3, CO_2, NO, NO_2, C_6H_6, and C_7H_8, at the same concentration.

Other types of gravimetric MOF sensors include microresonators and SAW devices. While microcantilevers utilize MOFs on a beam structure to detect frequency changes, microresonators use a fixed center paddle connected with beams. Hwang et al. proposed using ZIF-69, known for its high adsorption affinity toward CO_2, in a microresonator CO_2 sensor[88]. Dielectrophoresis methods were employed to directly assemble non-agglomerated ZIF-69 onto the resonator. This approach resulted in frequency shifts of 1 460.54, 2 246.66, 3 547.28, and 3 629.07 Hz for CO_2 concentrations of 1 300, 2 600, 3 900, and 5 200 ppm, respectively. This sensitive detection represents a 150-fold enhancement compared to bare Si resonators with identical dimensions. Additionally, the response and recovery times were less than 10 seconds, indicating fully reversible adsorption of the target material. The strong CO_2 adsorption properties of ZIF-69, driven by benzimidazolate linkers that facilitate dipole interactions, ensure high selectivity toward CO_2[89,90]. Paschke et al. proposed a method for fabricating high-performance MFU-4 SAW CO_2 gas sensors using in situ solvothermal growth of MFU-4 between two separate interdigitated transducers[91]. MFU-4 induces significant changes in acoustic wave velocity specifically toward CO_2, due to its pore size and adsorption affinity. The MFU-4 SAW sensor exhibited increasing sensor signals in the range of 10% to 100% CO_2, eventually saturating at higher concentrations, with τ_{90} of 3.52 seconds and τ_{10} of 4.86 seconds.

The integration of MOFs with gravimetric sensors has led to significant advancements in gas detection technologies. The

unique properties of MOFs, such as their high surface area, tunable pore sizes, and selective adsorption capabilities, contribute to the enhanced sensitivity and selectivity of gravimetric sensors, including microcantilever sensors, QCM sensors, microresonator sensors, and SAW sensors. These demonstrated successes highlight the potential utilization of MOFs in various gravimetric sensors for a variety of gases.

4.1.4. Optical MOF sensors. MOFs, with their highly ordered structures and extensive porosity, interact with gas molecules in ways that induce changes in light scattering, refraction, reflection, absorption, and luminescence[26]. These interactions make MOFs highly suitable for optical sensors, where their tunable porosity and adsorption properties can lead to sensitive detection of various gases through the observation of these optical changes. Dalstein et al. proposed a ZIF-8 nanopattern-based 2-D photonic crystal structure for detecting styrene gas (The schematically illustrated optical sensing method of this report is described in Figures 7(i) and (j). The gas response is determined by n factors after reflected beam from MOF surface between the air and analyte gas environment and described as Δn, which are changed according to gas molecule species and concentration[73]. ZIF-8 was synthesized via solution methods at room temperature and drop-cast onto a substrate, followed by a nanoimprinting process. The resulting ZIF-8 nanopatterns featured periodic nanogrooves with 780 nm spacing and 200 nm height and width. These periodic structures cause light diffraction at various angles when exposed to white light, which can be measured using a charge-coupled device (CCD) camera on a smartphone. The optical response of the ZIF-8 diffraction grating system was tested against styrene/water vapors with concentrations ranging from 1% to 10% (Figure 7(k)). Due to its hydrophobicity and flexible cage structure, ZIF-8 effectively adsorbs styrene, enabling the ZIF-8 optical styrene sensor to achieve selective uptake and a corresponding linear increase in its refractive index (RI). Notably, water vapor did not interfere with changes in the RI, as confirmed by the observation that vapor alone did not cause any variation in RI in the report. When analyzing the styrene uptake variations concerning the square root of time, the adsorption behavior was divided into two phases (Figure 7(l)): an initial fast uptake attributed to styrene adsorption on the surface of ZIF-8, followed by progressive penetration of styrene into the core of the ZIF-8 particles. The adsorption rates were highly dependent on the styrene concentration, enabling accurate styrene sensing in large concentration ranges even in humid conditions.

MOFs can also be integrated into optical fibers, which are valued for their flexibility and stability in various applications. Optical fibers, as waveguide-based sensors, can have their optical absorption adjusted and amplified through interactions with target gas analytes within porous MOFs. Zhu et al. proposed an HKUST-1 integrated optical fiber device for detecting nitrobenzene[92]. A single crystal of HKUST-1 was attached to the end of the optical fiber using solution synthesis at room temperature, and the interferogram shifts induced by the presence of nitrobenzene were used to measure its detection. Due to the strong adsorption of nitrobenzene by HKUST-1, facilitated by the interaction between the oxygen in the nitro group and Cu^{2+} ions, as well as the interaction between the aromatic component and the BTC^{3-} ligand in HKUST-1, the RI of the HKUST-1 loaded optical fiber changed upon nitrobenzene sensing[93]. Specifically, as HKUST-1 crystals adsorbed nitrobenzene, the effective RI of HKUST-1 increased, causing the interference spectra to shift to longer wavelengths. Kim et al. also developed a ZIF-8-coated optical fiber using a similar solution synthesis method[94]. When gases like CO_2 interact specifically with ZIF-8, the RI of ZIF-8 changes, leading to corresponding changes in transmitted light intensity. The intensity variance was directly correlated with the partial pressure of CO_2, thus, ZIF-8 optical fiber could detect a wide range of CO_2 concentrations from 10% to 100%, with less than 0.5% variation over 10 consecutive exposures.

Surface-enhanced Raman scattering (SERS) is another technique that can leverage MOFs to create microscale hotspots with high analyte adsorption capability. Phan-Quang et al. developed a stand-off SERS platform for detecting airborne molecules using a 3D Ag@MOF composite[95]. In this system, Ag nanocubes within the MOF serve as plasmonic nanoparticles, while the MOF provides adsorption sites for various airborne gas molecules and a platform for Ag encapsulation. With its flexible structure and optimal pore size, ZIF-8 effectively captures airborne gas molecules, enhancing the SERS intensity of embedded Ag nanocubes within its porous framework. The fabricated structures exhibited significantly larger and deeper SERS intensity, enabling highly sensitive gas detection. The Ag@ZIF-8 platform reached an intensity of over 5 000 counts within 30 seconds, while an Ag layer without MOF failed to reach 1 000 counts even after 60 seconds. According to the Lagergren pseudo-first-order adsorption kinetics, the Ag@ZIF-8 platform demonstrated the highest sorption constant, $k = 5.5 \times 10^{-2}$ s^{-1}. The large hotspots and high surface area of ZIF-8, combined with its adsorption capabilities, facilitated the rapid and quantitative detection of gases at ppb levels at 2–10 meters away. Furthermore, this platform could detect the fingerprints of multiple airborne polyaromatic hydrocarbons, including toluene and naphthalene, even under strong daylight background interference.

MOFs exhibit considerable potential in optical gas sensing applications due to their highly ordered structures, extensive porosity, and tunable adsorption properties, which facilitate significant interactions with gas molecules and lead to detectable changes in optical properties such as scattering, refraction, reflection, absorption, and luminescence. The examples discussed underscore the versatility and efficacy of MOFs in optical sensors, offering novel perspectives on the utilization of MOFs in various optical sensing technologies.

4.2. MOF-derivates as sensing layers

While some conductive MOFs have shown promising results in the electrochemical sensing of gaseous molecules, there are several limitations to their use in practical applications. First, the sensing sensitivity of MOFs is much lower than that of conventional SMOs. When exposed to target gas, the response in MOFs is less than one ($\Delta R/R_{air}$ or $\Delta C/C_{air}$), compared to the SMO sensing layer, which can exhibit changes greater than ten or even hundreds. Second, MOFs typically exhibit non-specific binding to various types of molecules due to their extremely high surface area, porosity, and dipole properties. Since electrochemical detection only measures a single electrical component, this non-selective binding can lead to false-positive signals. Third, MOFs tend to have lower reversibility compared to SMO materials. In SMOs, the detection of gaseous molecules occurs through catalytic oxidation-reduction reactions at high temperatures, while in MOFs, molecules are simply bound or captured in the pores with simple electron exchanges. Given these issues, direct use of MOF sensing layers in electrochemical sensing devices requires further functional modifications. Various efforts have been made to structurally modify MOFs, and we will briefly introduce some examples of these methods.

4.2.1. Thermal decomposition of MOFs. Thermal treatment of MOF crystals is the simplest method for modifying their structure. When heated above 300 °C in an oxygen environment, the organic linkers within the MOF lattice react with oxygen and decompose, leading to a collapse of the overall MOF crystallinity[96]. This process results in the production of N-doped carbon species containing electron-enriched functional groups, which enhance the reaction pathways of electrochemical sensing. The centered metal atoms are also oxidized and transformed into SMOs with much smaller grain sizes compared to those prepared by conventional hydrothermal reactions or deposition. The electron-depleted regions of this dimension usually align with the Debye length of the electrons, maximizing the sensitivity of the sensing materials[97]. Leveraging this chemistry, several groups have successfully demonstrated MOF-derived SMO gas sensors with performances superior to conventional techniques. For instance, Yuan et al. developed a hierarchically porous ZnO nanoarchitecture through the pyrolysis of a chip-level Zn-centered MOF layer at 400 °C for 3 hours in dry air (Figure 8(a))[98]. This nanoarchitecture features individual ZnO particles with diameters under 100 nm, forming a micro-mesoporous structure that provides a high surface area (53.4 $m^2 \cdot g^{-1}$). Further chemical bonding analysis via XPS revealed that these oxide particles contain a high number of oxygen vacancies, which can be modulated by varying the temperature ramping rate. These vacancies, created through defect engineering, provide unpaired electrons on the sensing layer, narrow the bandgap energy, and offer ample reactive sites for gas reactions. Using this material, they successfully detected 447 ppb of carbon monoxide gas at a 300 °C operating temperature. Similarly, Xia et al. reported the decomposition of ZIF-8 particles through in-situ annealing on a fast-ramping MEMS heater (60 $°C \cdot s^{-1}$)[99]. They heated the MOFs to 350 °C for two hours in dry air and confirmed that the resulting materials consisted of ZnO nanoparticles with grain sizes of 23.3 nm. These sensors demonstrated exceptional performance in detecting gaseous ethanol at a 250 °C operating temperature, with a response time shorter than 2 seconds and a detection limit of 1.2 ppb. Additionally, Ren et al. conducted pyrolysis on ZIF-8 at 500 °C in ambient air and demonstrated a highly sensitive NO_2 gas sensor with a detection limit in the tens of ppb range[100]. These studies offer valuable insights into achieving outstanding performances of SMO sensing materials through a simple thermal annealing process of MOFs above 300 °C.

4.2.2. SMO heterogeneous catalysts derived from MOFs. Anchoring noble metal species on oxide surfaces is a promising approach to enhance the performance of SMO gas sensors by facilitating effective reaction pathways, such as the Mars-van Krevelen or Langmuir-Hinshelwood mechanisms[104]. The size of the noble metal particles plays a crucial role in the performance of heterogeneous catalysts, but forming these particles on oxide surfaces requires well-controlled reaction conditions to prevent agglomeration and ensure higher uniformity. To address this challenge, Koo et al. utilized the nano-confined cages of MOF structures to suppress the excessive growth and agglomeration of particles (Figure 8(b))[101]. They mixed palladium precursors with ZIF-8 crystals, confining Pd^{2+} ions within the ZIF-8 pores. Subsequently, they added $NaBH_4$ to chemically reduce the Pd^{2+} ions, forming Pd nanoparticles within the ZIF-8 pores (Pd@ZIF-8). These particles were then combined with PVP and ammonium metatungstate hydrate and shaped into fiber structures using the electrospinning technique. Calcining these fibers at a high temperature (500 °C) for an hour resulted in the formation of WO3, ZnO, and 2–3 nanometers of PdO with high homogeneity (Pd@ZnO-WO_3). This material was used to detect gaseous toluene, a biomarker for lung cancer, successfully demonstrating a detection limit of 100 ppb. A distinctive feature of this sensing material is the p-n junction between the three oxides, which contributes to band bending. Likewise, recently, Sun et al. reported the creation of a unique 3D ZnO/Ag micro-octahedra structure by calcining MOF-5 and Ag precursors at 500 °C for one hour in air[105]. During the thermal treatment, the crystallinity of MOF-5 was completely decomposed while preserving its octahedral structure with the formation of Ag nanoparticles. This heterogeneous combination of SMO and noble metal contributed to high levels of oxygen vacancies and a catalytic spillover effect. Leveraging this unique material, the researchers demonstrated an ultrahigh sensing response of 293.8 to 10 ppm of gaseous triethylamine. This study highlights how the highly porous MOF structure and its nano-confinement capabilities can be leveraged to prepare unique heterogeneous sensing materials.

4.2.3. Templating and hybridization of nanomaterials and SMO. Despite the exceptional sensing capabilities of SMO materials, their high operating temperatures remain problematic due to excessive power consumption in devices. Over

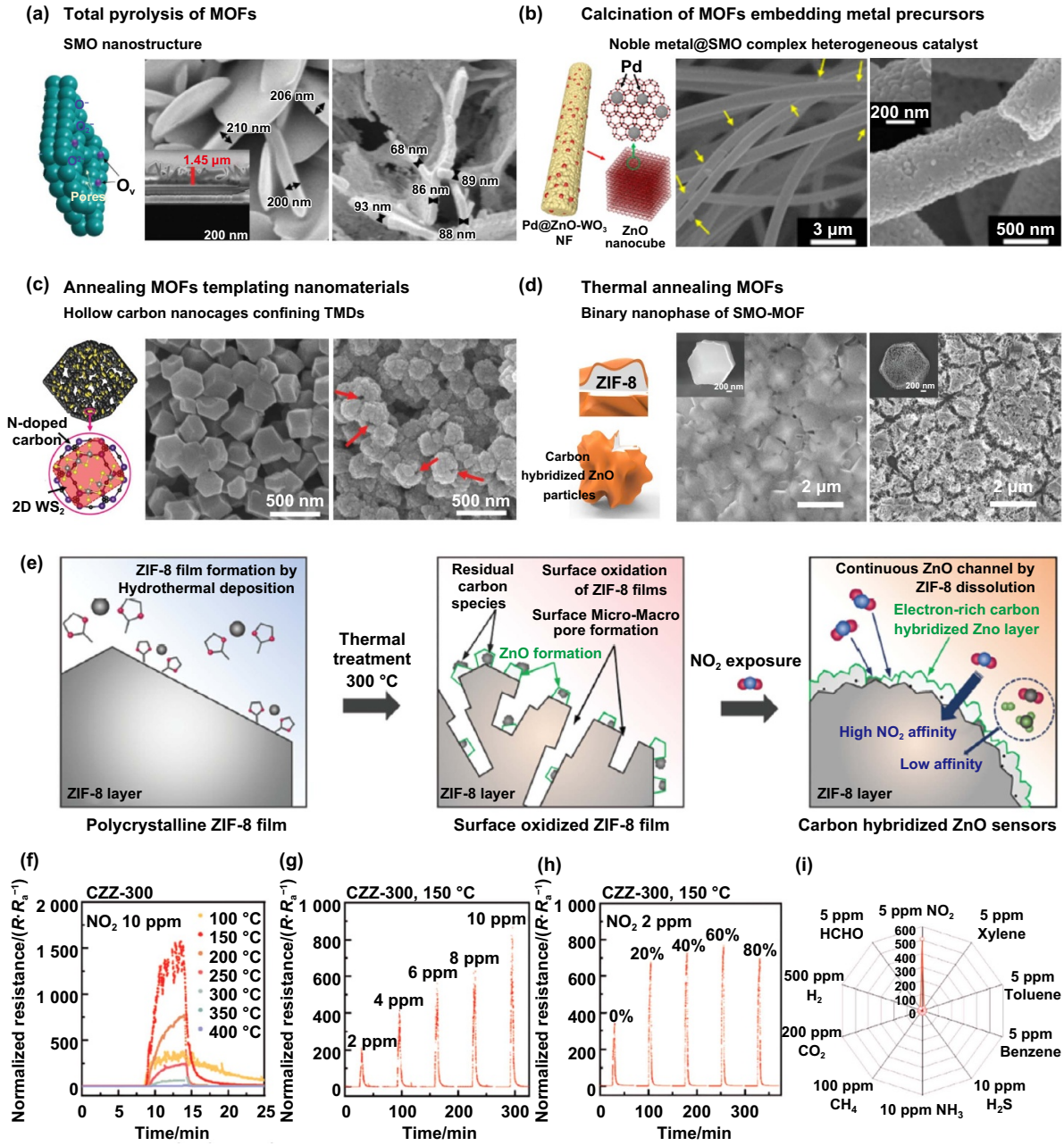

Figure 8. MOF-derived sensing materials. Utilizing thermal decomposition and confinement effect of porous MOFs for generating various nanostructures. (a) Hierarchical ZnO nanosheets prepared by the pyrolysis of MOF layers, Zn-centered MOF layer.[98] John Wiley & Sons. © 2019 WILEY-VCH Verlag GmbH & Co. KGaA, Weinheim. (b) Heterogeneous catalysts derived through the calcination of metal precursor-embedded MOF structures. Reprinted with permission from[101]. Copyright (2016) American Chemical Society. (c) Suppression of TMDs growth via the nano-confinement effect of MOF cages, with demonstration of an oxide/TMDs hybrid structure.[102] John Wiley & Sons. © 2018 WILEY-VCH Verlag GmbH & Co. KGaA, Weinheim. (d) Binary nanophase of oxide/MOF prepared by simple thermal annealing.[103] John Wiley & Sons. © 2023 Wiley-VCH GmbH. (e) Schematic representation of the formation of an oxides/MOF binary phase through thermal treatment and gaseous etching processes.[103] John Wiley & Sons. © 2023 Wiley-VCH GmbH. (f) Operating temperature-dependent response curve of an N-doped-carbon ZnO/ZIF-8 sensing layer (CZZ-300) against 10 ppm of NO_2 gas.[103] John Wiley & Sons. © 2023 Wiley-VCH GmbH. (g) Quantitative detection of NO_2 gases by the CZZ-300 sensor.[103] John Wiley & Sons. © 2023 Wiley-VCH GmbH. (h) Effect of humidity on the sensing capabilities of the CZZ-300 sensor.[103] John Wiley & Sons. © 2023 Wiley-VCH GmbH. (i) Gas sensing selectivity of the CZZ-300 sensor, showing a specific reaction toward NO_2 gas due to the strong affinity of the molecule to the ZIF-8 structure.[103] John Wiley & Sons. © 2023 Wiley-VCH GmbH.

the past few decades, room temperature detection of gaseous molecules has been extensively studied using 1-D and 2-D nanomaterials such as carbon nanotubes, graphene, and TMDs. Here, edge sites of those materials are known to be the primary active sites for gaseous molecule reactions, leading to significant efforts to increase these sites. In this context, Koo

et al. reported synthesizing a few layers of 2-D TMDs, specifically WS_2, by utilizing the nano-confined porous structures of ZIF-67 (Figure 8(c))[102]. They mixed WS_4^{2-} precursors with ZIF-67 to facilitate the spontaneous insertion of the precursors into the pores through electrostatic dipole interactions between the centered Co metals and the negatively charged WS_4^{2-}. The mixture was then pyrolyzed at 400 °C for two hours in an air atmosphere, followed by a reduction in a H_2/N_2 atmosphere at 700 °C for another two hours. Due to the confinement effect of the ZIF-67 layers, the growth of WS_2 was highly restricted, forming only a few layers. The ZIF-67 also decomposed under high temperatures, yielding Co_3O_4 with N-doped carbon species, which could contribute to forming electrical conducting channels and doping effects, enhancing the sensing capabilities of the devices. This sensor has been validated to detect 0.1 ppm of NO_2 gas at room temperature. This study also demonstrates the potential of MOF structures to fabricate nanomaterials/SMO hybrid sensing materials.

4.2.4. Binary nanophase of SMO-MOF. Although MOF-derived SMO sensing materials have shown significant enhancement of sensing capabilities, the high-temperature annealing conditions often lead to the collapse of the entire MOF structure, losing its advantages. Recently, Min et al. reported the development of N-doped carbon ZnO-ZIF binary structures that showed synergistic effect of the sensing capabilities of oxides with the high gas adsorption properties of ZIF-8 (Figure 8(d))[103]. In this study, they conducted annealing of ZIF-8 layer and simultaneously measured the electrical resistance across the material. They observed a rapid drop in overall resistance around 280 °C, implying the formation of conducting channel, ZnO and N-doped carbon species resulted from decomposition of ZIF-8 structure. They optimized the annealing temperature at 300 °C for one hour where the main part of the materials remained ZIF-8 crystallinity, but also had surface ZnO nanoparticles. In detail, while the XRD signals showed only peaks from ZIF-8 crystals, the EDX mapping indicated that 2 to 3 nm-sized ZnO nanoparticles were densely formed on the surfaces of the ZIF-8 layer. In-depth XPS data also revealed strong lattice oxygen on the surface of the material, suggesting that a ZnO layer covered the core ZIF-8. The XPS data also showed the presence of N-doped carbon residues that function as electron reservoirs for the ZnO species. Further exposure to NO_2 gas at 150 °C was determined to enhance the oxide lattice structures and etch unstable amorphous carbons, yielding well-connected conductive channels (Figure 8(e)). Using this material, they measured the sensing performance for gaseous NO_2 and optimized the operating temperature to 150 °C, where the response was calculated higher than 1 000 ($\Delta R/R_{air}$) (Figure 8(f)). Their quantitative analysis represented the detection limit of the sensor as 0.6 ppb (Figure 8(g)). Additionally, the response of CZZ-300 was enhanced by two-fold under humid conditions because the affinity for electron-withdrawing NO_2 molecules allowed them to displace pre-adsorbed water molecules, which are electron-donating species (Figure 8(h)). Furthermore, the unique nature of the ZIF-8 structure contributed to higher sensing selectivity, showing a high affinity for NO_2 compared to other industrial gases and VOCs (Figure 8(i)). This study is the first to demonstrate an organic-SMO-MOF hybrid structure derived from a single MOF structure through simple thermal treatment, opening new possibilities for future MOF-derived gas sensing materials.

4.3. MOFs as supportive components for sensor performance enhancement

Even though MOF can be an excellent candidate for sensing material, MOF also offers a rational approach to effectively enhance the "4S" of sensors: speed, selectivity, sensitivity, and stability as a supportive component, in the sensor system. MOFs are frequently coated onto various sensing layer, functioning as catalysts, molecular sieving membranes, hydrophobic layers, or often performing multiple roles simultaneously. The enhancement is primarily due to the unique characteristics of MOFs, such as their porosity, pore size, dimensionality, adjustable band gap, open metal sites, and the extensive variety of available MOF components[106–108]. This section focuses on examples and detailed mechanisms behind the supportive role of MOFs in various chemiresistive sensors, exploring how these properties contribute to performance enhancement. Additionally, it discusses the preparation methods of integrating MOFs into sensor devices.

4.3.1. Catalysts. The development of highly sensitive sensors capable of detecting extremely low concentrations is imperative in contemporary society. This capability opens new avenues for technological advancements in diverse fields and ensures early detection, enabling timely responses in situations such as disease diagnosis, industrial safety systems, and environmental monitoring. Consequently, the development of catalysts to enhance the sensitivity and detectability of sensors has been a primary focus for the past decades. Among various approaches, the catalytic role of MOFs in chemiresistive sensors offers a unique platform for enhancing sensor performance, owing to their highly ordered structures, tunable properties, and open metal sites. In chemical sensitization, MOFs facilitate catalytic activation and the spillover effect through abundant open metal sites, promoting reactions with target analytes. Additionally, MOFs offer customizable pore environments for tailored catalytic sensitization. Additionally, MOFs can offer electronic sensitization, which tunes the charge carrier concentration in the sensor during operation due to their finely tunable electronic properties depending on the sensing materials.

Lee et al. utilized ZIF-8 as a photocatalyst on UV-activated ZnO nanostructured sensors for sensitive and selective NO_2 sensing at room temperature (Figure 9(a))[109]. By using solvothermal reaction and in-situ growth on the substrate, 3D ZnO thin hierarchical nanostructures were converted to ZIF-8, covering the ZnO surface with a ZIF-8 layer. By controlling the thickness of ZnO and ZIF-8, the effect of ZIF-8 on photoactivation was optimized to improve sensitivity toward NO_2 gas. As a result, a 17-fold enhancement in gas response was achieved under UV illumination due to the solid interaction

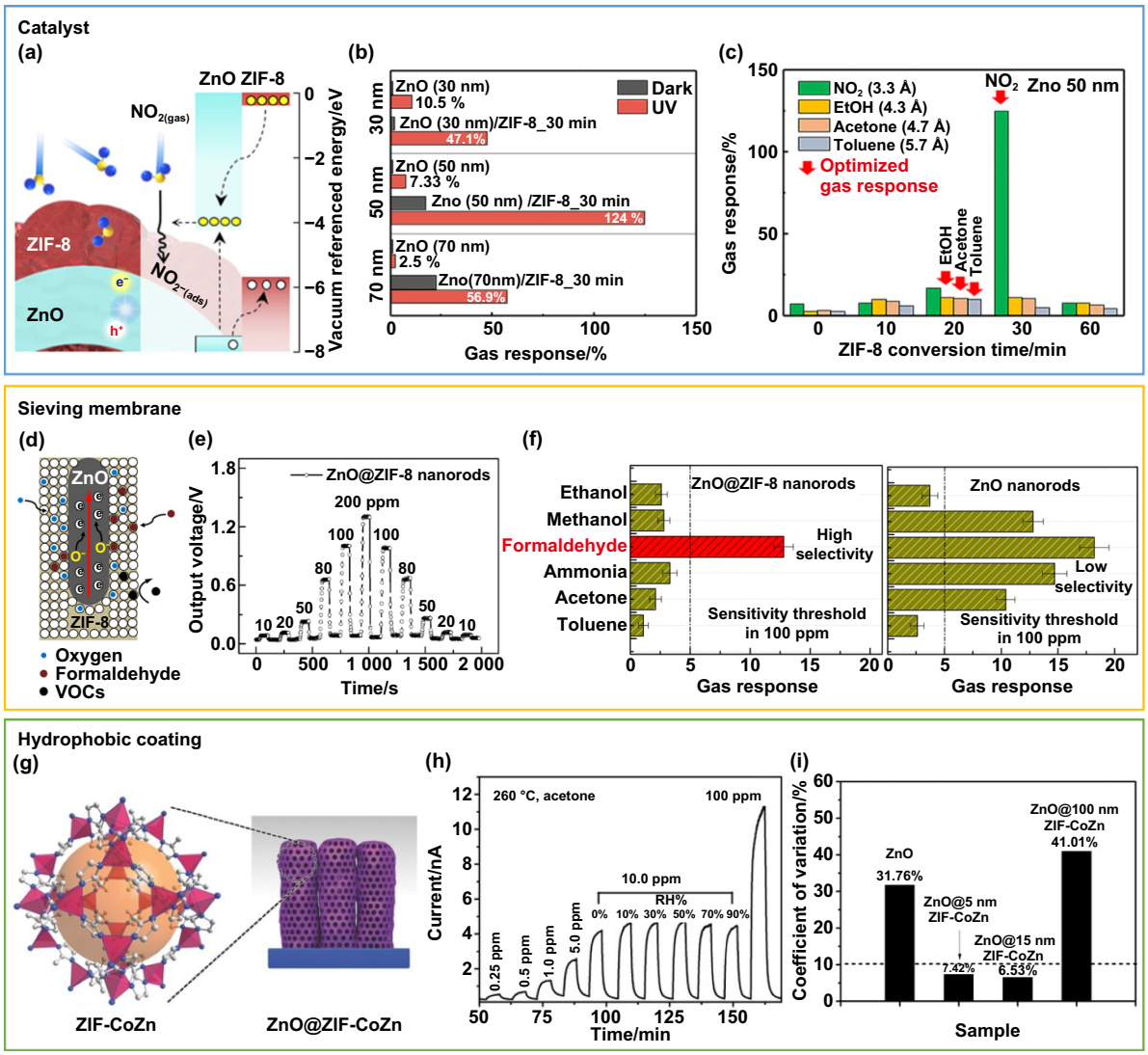

Figure 9. MOF as a supportive component for sensor performance enhancement. (a) Schematic illustration of ZIF-8 photocatalyst for ZnO NO_2 sensor. (b) Gas response of ZnO, ZIF-8@ZnO nanostructures under dark and UV light (365 nm) conditions at room temperature against 0.1 ppm NO_2. (c) Gas selectivity analysis of the ZIF-8@ZnO gas sensor against various VOCs. Reproduced from[109]. CC BY 4.0. (d) Schematic illustration of ZIF-8 as a sieving layer on ZnO formaldehyde sensor. (e) Sensing dynamics of ZIF-8@ZnO sensor against formaldehyde at concentrations from 10 to 200 ppm. (f) Selectivity of ZIF-8@ZnO and pristine ZnO sensor to 100 ppm of various VOCs at 300 °C. Reprinted with permission from[111]. Copyright (2016) American Chemical Society. (g) Schematic illustration of ZIF-CoZn hydrophobic coating on ZnO acetone sensor. (h) Sensing dynamics of ZIF-CoZn@ZnO sensor against acetone at the concentration range of 0.25 to 100 ppm under various humidity condition at 260 °C. (i) coefficient of variance of the sensors toward 10 ppm of acetone at 260 °C under varying humidity range from 0 to 90 RH%.[112] John Wiley & Sons. © 2016 WILEY-VCH Verlag GmbH & Co. KGaA, Weinheim.

between ZIF-8 and ZnO (Figure 9(b)). Specifically, while pristine 50 nm ZnO films achieved around 7.33%, ZIF-8 decorated 50 nm ZnO films achieved 124% against 0.1 ppm of NO_2 under UV illumination. As a result, the fabricated ZIF-8@ZnO nanostructures showed excellent sensitivity enhancement after appropriate ZIF-8 conversion and demonstrated exclusive selectivity through a selective molecular sieving effect, which will be discussed in a later section (Figure 9(c)). This enhancement is attributed to the photoactivation enhancement effect from the ZIF-8@ZnO composite, which induces effective interfacial charge transfer between the organic ligand and metal[110]. ZIF-8 effectively prevents interfacial charge recombination by transferring photo-activated electrons from the organic ligand to the Zn ion.

MOFs can also act as chemical catalysts instead of photocatalysts, providing more oxygen vacancies and additional reaction routes that generate larger charge differences upon gas introduction. Wu et al. utilized solvothermal in-situ growth of MOF to fabricate partially loaded ZIF-8@ZnO nanorods for sensitive H_2S detection[113]. Compared to pristine ZnO nanorod sensors, ZIF-8@ZnO nanorod sensors showed 15 times higher response toward 10 ppm H_2S at 25 °C and significant sensitivity enhancement across 1–10 ppm of H_2S. ZIF-8 on ZnO acts as a catalyst for H_2S reactions by providing

better gas adsorption, generating more oxygen vacancies compared to pristine ZnO, and offering intermediate reaction routes between ZIF-8 and H_2S. In detail, ZIF-8 induces the formation of ZnS and 2-methylimidazolate, which cause larger charge carrier concentration variation upon H_2S exposure. Alternatively, metal sites inside MOF cage structures can also induce chemical sensitization for better sensitivity and selectivity. Zhou et al. used solvothermal in-situ growth of MOF to fabricate Co-doped ZIF-71 on ZnO for an acetone sensor[114]. They utilized ZIF-71 as a framework for Co doping, which promotes the catalytic activation of oxygen and the decomposition of acetone[115]. As a result, ZIF-71(Co)@ZnO showed about 100 times higher gas response toward 50 ppb of acetone compared to undoped sensors at an optimal Co/Zn ratio. Similarly, ZIF-67 can directly alter the electronic properties of the sensing layer to further enhance sensitivity. DMello et al. reported ZIF-67@SnO_2 hybrid structures for enhancing sensitivity toward CO_2[116]. The coating of ZIF-67 on SnO_2 nanoparticles changed the electronic structures, involving partial electron transfer from imidazole to Sn and oxygen of SnO_2, and Co. These transfers provide better stabilization of CO_3^{2-} at the interfaces and increase CO_2 adsorption (an additional 23.5% CO_2 uptake). As a result, the fabricated hybrid ZIF-67@SnO_2 showed a 12-fold higher response compared to pristine SnO_2 toward 50% CO_2 and approximately 2 times higher response to 5 000 ppm CO_2. Additionally, the recovery time drastically decreased from 208 seconds to 22 seconds for 50% CO_2 and from 96 seconds to 25 seconds for 5 000 ppm CO_2.

MOFs play a crucial catalytic role in enhancing the performance of chemiresistive sensors. Their highly ordered structures, tunable properties, and open metal sites facilitate both chemical and electronic sensitization, leading to significant improvements in sensitivity and selectivity. Various studies, including those utilizing ZIF-8, ZIF-67, and ZIF-71(Co), have demonstrated substantial enhancements in gas response and selectivity for target analytes such as NO_2, H_2S, acetone, and CO_2. These advancements underscore the potential of MOF-based catalysts in developing highly sensitive and selective sensors for diverse applications.

4.3.2. Sieving membranes. Selectivity is essential in gas sensors to ensure accurate performance and prevent false alarms, particularly as their applications expand into the industrial, environmental, and medical fields. Various strategies have been developed to enhance selectivity, including chemical sensitization, electronic sensitization, heterojunction formation, multi-array electronic nose systems, and molecular sieving. Among these, molecular sieving offers a direct approach by filtering out interfering gases and allowing only the target analyte to reach the sensing layer for detection. Molecular sieving utilizes selective permeability of target analytes to the sensing layer, and its mechanism can be classified into two categories: physical and chemical sieving. Physical sieving uses precise pore sizes to permit only target analytes with smaller kinetic diameters to pass through while blocking larger molecules. For example, ZIF-8 has a pore size of 3.4 Å, which selectively allows small gases such as hydrogen (2.89 Å), formaldehyde (2.43 Å), and helium (2.6 Å) to pass through, while other competing gases are selectively excluded from the passage. Chemical sieving, on the other hand, involves specific interactions between the sieving material and gas molecules, where properties such as surface polarizability, acidity, reactivity, and magnetic susceptibility create strong binding sites that prevent non-target gases from accessing the sensing[81,117]. For instance, the organic linkers or metal nodes in MOFs can preferentially adsorb interfering gases, while unsaturated metal sites can coordinate with specific gas molecules, resulting in selective adsorption. Due to their tunable well-defined pore sizes, dimensionality, and exceptional stability, MOFs have emerged as promising sieving components for enhancing the selectivity of chemiresistive sensors, particularly in systems involving metal and semiconductor metal oxides, where spontaneous interactions with gas analytes are prevalent.

Physical sieving in MOFs typically requires precise control of pore size, which can be achieved by modifying the metal complexes or organic linkers in the framework. In detail, the length and structures of organic linkers and the charge and size of the metal ion can precisely control the pore size of MOFs for selective molecular sieving effect[118,119]. Tian et al. utilized hydrothermal methods to fabricate ZIF-8 for the selective permeation of formaldehyde among VOCs (Figure 9(d))[111]. The kinetic diameter of formaldehyde is 2.43 Å, while the kinetic diameters of other VOCs are 2.90 Å, 3.63 Å, 4.53 Å, 4.60 Å, and 5.25 Å for ammonia, methanol, ethanol, acetone, and toluene, respectively. Since ZIF-8's pore size is 3.4 Å, only formaldehyde can easily pass through the ZIF-8 and react with ZnO. The ZIF-8@ZnO showed sensitive detection toward a wide range of formaldehyde concentrations from 10 ppm to 200 ppm and demonstrated response and recovery speeds of about 16 seconds and 9 seconds, respectively, toward 100 pppm of formaldehyde (Figure 9(e)). This indicates that ZIF-8 did not impede the molecular movement of formaldehyde, allowing for sensitive and fast detection by ZnO. While achieving sensitive and fast detection, ZIF-8 effectively blocked reactions between ZnO and other VOCs, providing at least 4 times higher response for formaldehyde against other interfering VOCs (Figure 9(f)). Similarly, ZIF-8, fabricated using solvothermal in-situ growth on Pd/ZnO can also be utilized for selective H_2 sensors, as demonstrated by Weber et al. with ZIF-8@Pd/ZnO[120]. ZIF-8 covered Pd/ZnO nanowires, ensuring the permeation of H_2 with a 2.9 Å kinetic diameter while blocking interfering gases such as benzene, toluene, ethanol, and acetone. ZIF-8/Pd/ZnO nanowires showed gas responses of 3.2, 4.7, and 6.7 toward 10, 30, and 50 ppm of H_2, respectively, while noticeable responses were not observed toward interfering gases.

Beyond physical sieving, MOFs also enable chemical sieving, as their metal ions and the chemical properties of organic ligands facilitate selective adsorption, as shown by Yao et al.[68]. They designed a benzene sensor system with a sensing layer of conducting MOF Cu-HHTP and a sieving layer on top with Cu-5,10,15,20-tetrakis-(4-carboxyphenyl)porphyrin (TCPP). They used liquid-phase

epitaxy spray and solvothermal methods to fabricate two MOFs and utilized Van der Waals interactions to integrate into a sensor system. Without Cu-TCPP, Cu-HHTP shows a higher response toward NH_3 than benzene. However, with Cu-TCPP, which has abundant coordination-unsaturated Cu ions, resulting in a stronger interaction with NH_3. Thus, the interaction causes Jahn-Teller distortion, which blocks the NH_3 pathway. As a result, Cu-TCPP@Cu-HHTP showed a remarkable decrease in response toward NH_3 from 230% to 94%, while the response toward benzene increased from 134% to 153%. Additionally, the benzene sensor showed long-term stability up to 160 days and exhibited the highest sensitivity and selectivity among reported room temperature recoverable chemiresistive materials across 1–100 ppm of benzene. Likewise, Hwang et al. utilized Cu(BTC) to chemically adsorb CO for the selective detection of H_2[121]. By mixing Cu(BTC) with PDMS, the filter was placed in front of a commercial SnO_2 sensor. The MOF filter effectively prevents CO permeation to SMO sensors, having an adsorption efficiency of up to 62.38% at 20 ppm CO with a 20 wt% Cu(BTC)/polydimethylsiloxane (PDMS) filter and selectivity enhancement up to 2.7 times. This selectivity is attributed to the presence of Cu in Cu(BTC), which facilitates the adsorption of CO, CH_4, CO_2, and VOCs. Finally, due to MOF's superior mechanical and chemical stability, the filter shows excellent reproducibility and long-term stability with under 5% standard deviation between five different filters and stable performance for 3 months.

MOFs, with their various pore sizes, dimensionalities, and adsorption surface properties, provide a rational system to control the physical and chemical adsorption of various interfering gases and enhance selectivity performance without sacrificing other performances such as sensitivity, speed, and stability. This overcomes conventional limitations of various sensors, especially SMO sensors, and opens new avenues for high-performing gas sensors that can operate in diverse environments and situations.

4.3.3. Hydrophobic-coating materials. Stability is an indispensable parameter that must be ensured for industrialization and practical application in real life. Among various environmental effects, humidity has posed significant challenges for more than 70 years as it causes critical performance degradation, electrical property changes, and baseline drifting in chemiresistive sensors, especially in SMO sensors[122−124]. When water molecules reach the sensor surface, they break down into hydrogen and hydroxyl ions and adsorb onto the sensor surface, with excess molecules adsorbing through hydrogen bonding. Additionally, the presence of water molecules during detection often competes with the target analyte and occupies active chemical sites, reducing the rate of target gas reaction and recovery. Here, MOFs can play a vital role in preventing water adsorption on the sensor surface through a molecular sieving effect or chemical adsorption with water molecules before they reach the sensor layer. Although the general mechanism is similar to the previous MOF sieving section, this section focuses on stability enhancement against humidity, discussing the stability enhancement from water molecules in detail.

Yao et al. reported ZIF-CoZn@ZnO to mitigate the effects of water molecules during gas response with acetone (Figure 9(g))[112]. Solvothermal in-situ growth of ZIF-CoZn on ZnO effectively acts as a filtration membrane, allowing acetone to permeate while preventing water molecules due to its hydrophobic nature. As shown in Figure 9(h), the current change toward 10 ppm of acetone under various humidity environments (0–90 RH%) demonstrated sensitive detection without performance degradation. To evaluate the effect of ZIF-CoZn in preventing humidity interference, the coefficient of variation was also assessed (Figure 9(i)). The coefficient of variation represents the ratio between the standard deviation of response and the average response value under different humidity conditions, with a higher coefficient indicating worse anti-interference performance. While ZnO nanowire arrays showed a variation as high as 31.76%, ZIF-CoZn coated ZnO nanowires exhibited only 7.42% variation for 5 nm coating and further decreased to 6.53% for 15 nm coating. However, with 100 nm coating, the variation increased to 41.01%, attributed to the competing response of the ZnO core and the p-type CoO_x cover. As ZIF-67 (Co) shows poor thermal stability, the thickness increment of the ZIF-CoZn coating causes more oxidation of ZIF (Co) to CoO_x nanoparticles at the operation temperature of 260 °C. Consequently, the response becomes p-type, inducing resistance increases similar to water molecules upon acetone introduction. However, with MOF thickness control, ZIF-CoZn provides a rational way to inhibit water molecule interaction, while maximizing its reaction with acetone. Co and Zn in ZIF provide excellent catalytic effects to activate oxygen molecules and generate active oxygen species for the reaction with acetone (response enhancement ∼20 times, detection limit enhancement ∼2 times). Similarly, Qu et al. introduced porous CoBDC and PDMS on $CoSnO_3$ for humidity-independent gas detection[125]. CoBDC was applied to $CoSnO_3$ using thermal reaction as the initial coating layer, followed by a common hydrophobic PDMS polymer coating, achieving approximately 120° water contact angles. The fabricated CoBDC/PDMS@$CoSnO_3$ sensor showed within 10% standard deviation limit from the normalized response for 5 ppm H_2S, 100 ppm NH_3, ethanol, xylene, and Trimethylamine at 160 °C against 0–90 RH% humidity levels. Additionally, the MOF-based PDMS coating is viable for ZnO and SnO_2, primary n-type SMO materials, preserving their performance. Here, CoBDC acts as a supplementary water sieving layer and catalyst. Zhou et al. reported three-dimensional ordered microporous (3DOM) ZIF-CoZn@$ZnCo_xO$ sensors for a sensitive, humidity resistant sensor[67]. In detail, 3D structures were coated with MOF using thermal reaction with imidazole ligand solution. Fabricated ZIF-CoZn@$ZnCo_xO$ showed approximately 96.2° water contact angles and maintained 93.1% of the initial response after 90 days. This can be attributed to the mechanically robust, water-resistant MOF filters. For anti-humidity tests in the RH range of 35%–75%, the response under 75 RH%

to 5 ppm of H_2S reached 62% of the original value, exhibiting good humidity resilience. In addition, although discussed in previous sections, various MOFs served as water filter layers, providing resistance to humidity during sensing and storage, as illustrated by Wu et al. with ZIF-8 (138° water contact angle)[113], and Hwang et al. with MIL-160/PDMS filter (over 70% RH adsorption efficiency)[121].

MOF hydrophobic coatings significantly enhance the stability and performance of chemiresistive sensors by mitigating the adverse effects of humidity. By providing effective molecular sieving and chemical adsorption properties, MOFs prevent water molecules from interfering with sensor surfaces, thus maintaining sensitivity and selectivity. MOFs have demonstrated substantial improvements in sensor performance, including enhanced response times, recovery speeds, and resilience to humidity-induced degradation. These advancements underscore the potential of MOF coatings in developing reliable, high-performance gas sensors for various humid industrial and environmental applications.

5. Conclusions and outlooks

Significant progress has been made over the years in developing sensors for the efficient and effective detection of toxic gases, greenhouse gases, volatile organic compounds, and inflammable gases. While various materials, including SMO have been explored, MOFs have emerged as promising candidates due to their superior tunability in structure and chemical composition. Specifically, their highly ordered porous frameworks, formed from diverse metal ions and organic ligands, enable a wide range of chemical, electronic, and structural properties. Their versatile functionality allows for strong interactions with gas molecules, making MOFs a compelling choice for high-performing gas sensor applications. MOFs have been incorporated into sensor components using techniques such as drop-casting, tape-casting, spin-coating, template-mediated synthesis, interfacial synthesis, Langmuir-Blodgett deposition, electrochemical deposition, and exfoliation. Fabricated MOF gas sensors exhibit sensitive changes in electrical resistance, capacitance, mass, and optical properties after gas adsorption, attributed to their high porosity and selective adsorption capabilities. Moreover, MOFs can enhance sensor performance by introducing hydrophobicity, extending charge transport pathways, and integrating catalysts into their pores through combinations of different organic linkers or metal nodes. This paper has provided a detailed discussion of recent advances in MOF-based gas sensors, their working principles, and fabrication methods. Maximizing the potential of various MOFs could drive significant advancements in gas sensor technology with broad implications across numerous industries. However, despite notable progress, there remains substantial room for improvement to meet its expectations. Further endeavors are needed to focus on the following issues.

- First, more emphasis should be placed on the processability and homogeneity of MOF fabrication, which has often been overlooked. MOF production often involves complex fabrication processes that require high pressure and temperature, making it crucial to consider scalable manufacturing methods and commercial viability along with its homogeneity for industrial-level sensor production. Additionally, the cost of production and its environmental impact must not be overlooked, necessitating careful monitoring through comprehensive life cycle assessments or green synthesis methods development[126–128]. As variations in structure and composition during the scale-up process can significantly affect their sensing properties, more efforts should be made to bridge the gap between academia and industry. Artificial intelligence-assisted fabrication processes could be implemented to precisely control synthesis conditions on a large scale, and alternative manufacturing routes could provide solutions for broader industrial applications of MOF-based sensors[129,130].
- Second, although various fabrication methods have been proposed, MOF sensors predominantly rely on solvothermal synthesis and subsequent drop-casting processes for sensor fabrication. Exploring alternative fabrication techniques could unlock untapped advantages and properties, as the unique characteristics of MOFs are closely linked to their fabrication methods. Structural, dimensional, compositional, and alignment variations could further diversify MOF-based sensors and enhance their sensing performance in various applications. For instance, alternative MOF fabrication techniques—such as microcontact printing, electrochemical deposition, seeding patterning, ceramic conversion, ink-jet and spray coating, nanoimprinting, photolithography, and electron-beam lithography—enable a broad range of structural variations and precise patterning. These approaches pave the way for the development of high-performance gas sensors with unique functionalities[131–133].
- Third, the stability of MOF-based sensors requires further attention. As noted in previous research, MOFs exhibit irreversible gas adsorption during detection, leading to baseline drift and incomplete recovery. Enhanced efforts, such as platform and MOF engineering, should be further pursued to achieve fully reversible gas detection. In detail, material-based strategies that include metal ion, ligand substitution in MOFs and heterostructures, or external sensor platforms incorporating UV light or heat-assisted systems can induce stable and reversible sensing dynamics that overcome conventional limitations[63,134–138]. Additionally, addressing the effects of environmental fluctuations, such as temperature and humidity, is essential to broaden the range of applications for MOF-based sensors.
- Finally, MOFs hold significant potential as template materials for fabricating highly porous nanostructures. Their tunability provides flexibility over metal sites, pore sizes, dimensions, and metal encapsulation, enabling the creation of various porous nanostructures through simple thermal treatment. This approach combines the advantages of MOFs with relatively straightforward fabrication methods to produce 3D nanostructures with superior performance across a wide range of applications. As detailed in Figure 8, thermal

annealing of MOF produces a variety of structures, including pristine porous SMO, MOF-SMO heteronanostructures, and bilayer hybrid MOF-SMO configurations with numerous catalyst embedments. Consequently, further exploration of MOF-based nanostructures and their combinations is necessary[98,101 – 103].

In conclusion, MOFs offer distinct advantages in various gas sensor systems. By leveraging these benefits while addressing the outlined endeavors, the full potential of MOFs can be realized, leading to their successful application in a wide array of real-world scenarios.

This review aims to provide a comprehensive introduction and insights into MOF-based gas sensors and their fabrication, offering new perspectives to guide future developments in this promising field.

Acknowledgments

This work was supported by the National Research Foundation of Korea (NRF) grant funded by the Korean government (MSIT) (RS-2024-00333650). This research was supported by basic science research program through the National Research Foundation of Korea funded by the Ministry of Education (NRF-2019R1A6A1A11055660). This work was supported by the Technology Innovation Program("20013621", Center for Super Critical Material Industrial Technology) funded By the Ministry of Trade, Industry & Energy(MOTIE, Korea). This research was supported by Strategic Networking & Development Program funded by the Ministry of Science and ICT through the National Research Foundation of Korea(RS-2023-00268523).

ORCID iDs

Soon Hyeong So 0000-0002-5536-7366
Kyu Hyoung Lee 0000-0001-6843-6706
Dae Woo Kim 0000-0001-6533-8086

References

[1] Li J Z, Li Y Q and Zeng W. 2024. Gas sensing technology as the key to safety warning of lithium-ion battery: recent advance. *Sens. Actuators A* **365**, 114890.
[2] Kishore S C, Perumal S, Atchudan R, Alagan M, Sundramoorthy A K, Ramalingam S, Manoj D and Sambasivam S. 2024. A critical review on black phosphorus and its utilization in the diverse range of sensors. *Sens. Actuators A* **377**, 115719.
[3] Majhi S M, Mirzaei A, Kim H W, Kim S S and Kim T W. 2021. Recent advances in energy-saving chemiresistive gas sensors: a review. *Nano Energy* **79**, 105369.
[4] Ishihara T, Kometani K, Mizuhara Y and Takita Y. 1993. Capacitive-type gas sensor for the selective detection of carbon dioxide. *Sens. Actuators B* **13**, 470–472.
[5] Lee J, Choi N-J, Lee H-K, Kim J, Lim S Y, Kwon J Y, Lee S M, Moon S E, Jong J J and Yoo D J. 2017. Low power consumption solid electrochemical-type micro CO_2 gas sensor. *Sens. Actuators B* **248**, 957–960.
[6] Jalkanen T, Tuura J, Mäkilä E and Salonen J. 2010. Electro-optical porous silicon gas sensor with enhanced selectivity. *Sens. Actuators B* **147**, 100–104.
[7] Imai Y, Tadaki D, Ma T, Kimura Y, Hirano-Iwata A and Niwano M. 2017. Response characteristics of hydrogen gas sensor with porous piezoelectric poly(vinylidene fluoride) film. *Sens. Actuators B* **247**, 479–489.
[8] Tardy P, Coulon J-R, Lucat C and Menil F. 2004. Dynamic thermal conductivity sensor for gas detection. *Sens. Actuators B* **98**, 63–68.
[9] Pyo S, Lee K, Noh T, Jo E and Kim J. 2019. Sensitivity enhancement in photoionization detector using microelectrodes with integrated 1D nanostructures. *Sens. Actuators B* **288**, 618–624.
[10] Fanget S, Hentz S, Puget P, Arcamone J, Matheron M, Colinet E, Andreucci P, Duraffourg L, Myers E and Roukes M L. 2011. Gas sensors based on gravimetric detection—a review. *Sens. Actuators B* **160**, 804–821.
[11] Hong S, Wu M L, Hong Y, Jeong Y, Jung G, Shin W, Park J, Kim D, Jang D and Lee J-H. 2021. FET-type gas sensors: a review. *Sens. Actuators B* **330**, 129240.
[12] Zhang J, Liu L, Yang Y, Huang Q W, Li D L and Zeng D W. 2021. A review on two-dimensional materials for chemiresistive- and FET-type gas sensors. *Phys. Chem. Chem. Phys.* **23**, 15420–15439.
[13] Padha B, Verma S, Mahajan P, Sundramoorthy A K and Arya S. 2023. An insight into the wearable technologies based on novel hybrid piezoelectric-triboelectric nanogenerators. *Energy Technol.* **11**, 2300224.
[14] Sharma A, Singh A, Gupta V, Sundramoorthy A K and Arya S. 2023. Involvement of metal organic frameworks in wearable electrochemical sensor for efficient performance. *Trends Environ. Anal. Chem.* **38**, e00200.
[15] Annamalai J, Murugan P, Ganapathy D, Nallaswamy D, Atchudan R, Arya S, Khosla A, Barathi S and Sundramoorthy A K. 2022. Synthesis of various dimensional metal organic frameworks (MOFs) and their hybrid composites for emerging applications—a review. *Chemosphere* **298**, 134184.
[16] Lin J C, Kilani M and Mao G Z. 2023. Recent advances in integrating 1D nanomaterials into chemiresistive gas sensor devices. *Adv. Mater. Technol.* **8**, 2202038.
[17] Jiao L, Seow J Y R, Skinner W S, Wang Z U and Jiang H-L. 2019. Metal–organic frameworks: structures and functional applications. *Mater. Today* **27**, 43–68.
[18] Wang S, Fu Y, Wang T, Liu W S, Wang J, Zhao P, Ma H P, Chen Y, Cheng P and Zhang Z J. 2023. Fabrication of robust and cost-efficient Hoffmann-type MOF sensors for room temperature ammonia detection. *Nat. Commun.* **14**, 7261.
[19] Peng X Y, Wu X H, Zhang M M and Yuan H Y. 2023. Metal–organic framework coated devices for gas sensing. *ACS Sens.* **8**, 2471–2492.
[20] Guo L Z, Sun J F, Wei J X, Liu Y, Hou L R and Yuan C Z. 2020. Conductive metal-organic frameworks: recent advances in electrochemical energy-related applications and perspectives. *Carbon Energy* **2**, 203–222.
[21] Koo W-T, Jang J-S and Kim I-D. 2019. Metal-organic frameworks for chemiresistive sensors. *Chem* **5**, 1938–1963.
[22] Mu J L, Zhong X, Dai W, Pei X, Sun J, Zhang J Y, Luo W J and Zhou W. 2022. Metal-organic framework assembled on oriented nanofiber arrays for field-effect transistor and gas sensor-based applications. *Molecules* **27**, 2131.
[23] Wang X K, Xu X Y, Zhou T T and Zhang T. 2024. Nanoscale MOF-74-based QCM gas sensor for CO_2 detection at room temperature. *Sens. Actuators B* **413**, 135874.
[24] Shen Y W, Tissot A and Serre C. 2022. Recent progress on MOF-based optical sensors for VOC sensing. *Chem. Sci.* **13**, 13978–14007.

[25] Jo Y-M, Jo Y K, Lee J-H, Jang H W, Hwang I-S and Yoo D J. 2023. MOF-based chemiresistive gas sensors: toward new functionalities. *Adv. Mater.* **35**, 2206842.
[26] Yuan H Y, Li N X, Fan W D, Cai H and Zhao D. 2022. Metal-organic framework based gas sensors. *Adv. Sci.* **9**, 2104374.
[27] Li H-Y, Zhao S-N, Zang S-Q and Li J. 2020. Functional metal-organic frameworks as effective sensors of gases and volatile compounds. *Chem. Soc. Rev.* **49**, 6364–6401.
[28] Guo X Q, Wang L, Wang L, Huang Q, Bu L and Wang Q. 2023. Metal-organic frameworks for food contaminant adsorption and detection. *Front. Chem.* **11**, 1116524.
[29] Sezgin P, Gulcay-Ozcan E, Vučkovski M, Bondžić A M, Erucar I and Keskin S. 2025. Biomedical applications of metal-organic frameworks revisited. *Ind. Eng. Chem. Res.* **64**, 1907–1932.
[30] Huang X Y, Gong Z J and Lv Y. 2022. Advances in metal-organic frameworks-based gas sensors for hazardous substances. *Trends Analyt. Chem.* **153**, 116644.
[31] Shirbeeny W and Mahmoud W E. 2014. Synthesis and characterization of transparent optical gas sensor device made of indium oxide pyramid like nanoarchitectures. *Sens. Actuators B* **191**, 102–107.
[32] Xu H, Wu P, Zhu C, Elbaz A and Gu Z Z. 2013. Photonic crystal for gas sensing. *J. Mater. Chem. C* **1**, 6087–6098.
[33] Tabassum R and Kant R. 2020. Recent trends in surface plasmon resonance based fiber–optic gas sensors utilizing metal oxides and carbon nanomaterials as functional entities. *Sens. Actuators B* **310**, 127813.
[34] Hromadka J, Tokay B, James S, Tatam R P and Korposh S. 2015. Optical fibre long period grating gas sensor modified with metal organic framework thin films. *Sens. Actuators B* **221**, 891–899.
[35] Wu J Y, Zhang W Y, Wang Y, Li B H, Hao T, Zheng Y B, Jiang L Z, Chen K X and Chiang K S. 2020. Nanoscale light-matter interactions in metal-organic frameworks cladding optical fibers. *Nanoscale* **12**, 9991–10000.
[36] Wu J W et al. 2020. On-chip optical gas sensors based on group-IV materials. *ACS Photonics* **7**, 2923–2940.
[37] Li H L, Eddaoudi M, O'Keeffe M and Yaghi O M. 1999. Design and synthesis of an exceptionally stable and highly porous metal-organic framework. *Nature* **402**, 276–279.
[38] Chui S S-Y, Lo S M-F, Charmant J P H, Orpen A G and Williams I D. 1999. A chemically functionalizable nanoporous material $[Cu_3(TMA)_2(H2O)_3]_n$. *Science* **283**, 1148–1150.
[39] Millange F, Serre C and Férey G. 2002. Synthesis, structure determination and properties of MIL-53as and MIL-53ht: the first Cr^{III} hybrid inorganic-organic microporous solids: $cr^{III}(OH)\cdot\{O_2C\text{-}C_6H_4\text{-}CO_2\}\cdot\{HO_2C\text{-}C_6H_4\text{-}CO_2H\}_x$. *Chem. Commun.* **2**, 822–823.
[40] Cavka J H, Jakobsen S, Olsbye U, Guillou N, Lamberti C, Bordiga S and Lillerud K P. 2008. A new zirconium inorganic building brick forming metal organic frameworks with exceptional stability. *J. Am. Chem. Soc.* **130**, 13850–13851.
[41] Park K S, Ni Z, Côté A P, Choi J Y, Huang R, Uribe-Romo F J, Chae H K, O'Keeffe M and Yaghi O M. 2006. Exceptional chemical and thermal stability of zeolitic imidazolate frameworks. *Proc. Natl Acad. Sci. USA* **103**, 10186–10191.
[42] Huang X-C, Lin -Y-Y, Zhang J-P and Chen X-M. 2006. Ligand-directed strategy for zeolite-type metal-organic frameworks: zinc(II) imidazolates with unusual zeolitic topologies. *Angew. Chem., Int. Ed.* **45**, 1557–1559.
[43] Caskey S R, Wong-Foy A G and Matzger A J. 2008. Dramatic tuning of carbon dioxide uptake via metal substitution in a coordination polymer with cylindrical pores. *J. Am. Chem. Soc.* **130**, 10870–10871.
[44] Kim M, Pander M and Moon H R. 2024. Advancing metal-organic framework designs for room-temperature chemiresistive gas sensors. *ACS Appl. Electron. Mater.* **6**, 3024–3038.
[45] Xie L S, Skorupskii G and Dincă M. 2020. Electrically conductive metal–organic frameworks. *Chem. Rev.* **120**, 8536–8580.
[46] Li W H, Deng W H, Wang G E and Xu G. 2020. Conductive MOFs. *EnergyChem* **2**, 100029.
[47] Sun L, Campbell M G and Dincă M. 2016. Electrically conductive porous metal–organic frameworks. *Angew. Chem., Int. Ed.* **55**, 3566–3579.
[48] Zhu B J, Wen D S, Liang Z B and Zou R Q. 2021. Conductive metal-organic frameworks for electrochemical energy conversion and storage. *Coord. Chem. Rev.* **446**, 214119.
[49] Small L J and Nenoff T M. 2017. Direct electrical detection of iodine gas by a novel metal-organic-framework-based sensor. *ACS Appl. Mater. Interfaces* **9**, 44649–44655.
[50] Assen A H, Belmabkhout Y, Adil K, Bhatt P M, Xue D-X, Jiang H and Eddaoudi M. 2015. Ultra-tuning of the rare-earth fcu-MOF aperture size for selective molecular exclusion of branched paraffins. *Angew. Chem., Int. Ed.* **54**, 14353–14358.
[51] Li L B, Vizuet J P, McCandless G T and Balkus K J Jr. 2023. Controlling pore size and interlayer space by ring rotation and electron-withdrawing effects in a 2D MOF. *Polyhedron* **230**, 116211.
[52] Nodera A and Aikawa S. 2024. In_2O_3-based thin-film transistors with a (400) polar surface for CO_2 gas detection at 150°C. *Mater. Sci. Eng.* **299**, 117034.
[53] Wang L, Teleki A, Pratsinis S E and Gouma P I. 2008. Ferroelectric WO_3 nanoparticles for acetone selective detection. *Chem. Mater.* **20**, 4794–4796.
[54] Kökçam-Demir Ü, Goldman A, Esrafili L, Gharib M, Morsali A, Weingart O and Janiak C. 2020. Coordinatively unsaturated metal sites (open metal sites) in metal-organic frameworks: design and applications. *Chem. Soc. Rev.* **49**, 2751–2798.
[55] Xie L-H, Xu -M-M, Liu X-M, Zhao M-J and Li J-R. 2020. Hydrophobic metal–organic frameworks: assessment, construction, and diverse applications. *Adv. Sci.* **7**, 1901758.
[56] Kim J-O, Koo W-T, Kim H, Park C, Lee T, Hutomo C A, Choi S Q, Kim D S, Kim I-D and Park S. 2021. Large-area synthesis of nanoscopic catalyst-decorated conductive MOF film using microfluidic-based solution shearing. *Nat. Commun.* **12**, 4294.
[57] Ellis J E, Crawford S E and Kim K-J. 2021. Metal-organic framework thin films as versatile chemical sensing materials. *Mater. Adv.* **2**, 6169–6196.
[58] Homayoonnia S and Zeinali S. 2016. Design and fabrication of capacitive nanosensor based on MOF nanoparticles as sensing layer for VOCs detection. *Sens. Actuators B* **237**, 776–786.
[59] Li M Y and Dincă M. 2014. Selective formation of biphasic thin films of metal-organic frameworks by potential-controlled cathodic electrodeposition. *Chem. Sci.* **5**, 107–111.
[60] Wu X H et al. 2024. Solution-processable $Ni_3(HITP)_2$/MXene heterostructures for ppb-level gas detection. *J. Mater. Chem. A* **12**, 17382–17394.
[61] Wu X H et al. 2024. Solution-processable MOF-on-MOF system constructed via template-assisted growth for ultratrace H_2S detection. *Angew. Chem., Int. Ed.* **63**, e202410411.
[62] Lee J-H, Nguyen T T T, Nguyen L H T, Phan T B, Kim S S and Doan T L H. 2021. Functionalization of zirconium-based metal–organic frameworks for gas sensing applications. *J. Hazard. Mater.* **403**, 124104.

[63] Jo Y-M, Lim K, Yoon J W, Jo Y K, Moon Y K, Jang H W and Lee J-H. 2021. Visible-light-activated type II heterojunction in Cu_3(hexahydroxytriphenylene)$_2$/Fe_2O_3 hybrids for reversible NO_2 sensing: critical role of π-π^* transition. *ACS Cent. Sci.* **7**, 1176–1182.

[64] Murugesan T, Kumar R R, Ranjan A, Lu M-Y and Lin H-N. 2024. Fabrication of large-area Au nanoparticle decorated ZnO@ZIF-8 core-shell heterostructure nanorods for ppb-level NO_2 gas sensing at room temperature. *Sens. Actuators B* **402**, 135106.

[65] Campbell M G, Liu S F, Swager T M and Dincă M. 2015. Chemiresistive sensor arrays from conductive 2D metal-organic frameworks. *J. Am. Chem. Soc.* **137**, 13780–13783.

[66] Meng Z, Aykanat A and Mirica K A. 2019. Welding metallophthalocyanines into bimetallic molecular meshes for ultrasensitive, low-power chemiresistive detection of gases. *J. Am. Chem. Soc.* **141**, 2046–2053.

[67] Zhou Q Q, Yang L, Kan Z T, Lyu J K, Wang M X, Dong B, Bai X, Chang Z Y, Song H W and Xu L. 2022. Diverse scenarios selective perception of H_2S via cobalt sensitized MOF filter membrane coated three-dimensional metal oxide sensor. *Chem. Eng. J.* **450**, 138014.

[68] Yao M-S, Xiu J-W, Huang Q-Q, Li W-H, Wu -W-W, Wu A-Q, Cao L-A, Deng W-H, Wang G-E and Xu G. 2019. Van der Waals heterostructured MOF-on-MOF thin films: cascading functionality to realize advanced chemiresistive sensing. *Angew. Chem., Int. Ed.* **58**, 14915–14919.

[69] Ghanbarian M, Zeinali S and Mostafavi A. 2018. A novel MIL-53(Cr-Fe)/Ag/CNT nanocomposite based resistive sensor for sensing of volatile organic compounds. *Sens. Actuators B* **267**, 381–391.

[70] Ishihara T and Matsubara S. 1998. Capacitive type gas sensors. *J. Electroceram.* **2**, 215–228.

[71] Zhai Z Y, Zhang X L, Hao X K, Niu B and Li C J. 2021. Metal–organic frameworks materials for capacitive gas sensors. *Adv. Mater. Technol.* **6**, 2100127.

[72] Fernandez E, Saiz P G, Peřinka N, Wuttke S and Fernández de Luis R. 2021. Printed capacitive sensors based on ionic liquid/metal-organic framework composites for volatile organic compounds detection. *Adv. Funct. Mater.* **31**, 2010703.

[73] Chernikova V, Yassine O, Shekhah O, Eddaoudi M and Salama K N. 2018. Highly sensitive and selective SO_2 MOF sensor: the integration of MFM-300 MOF as a sensitive layer on a capacitive interdigitated electrode. *J. Mater. Chem. A* **6**, 5550–5554.

[74] Savage M et al. 2016. Selective adsorption of sulfur dioxide in a robust metal–organic framework material. *Adv. Mater.* **28**, 8705–8711.

[75] Xia B Z et al. 2022. Single-Crystal capacitive sensors with micropatterned electrodes via space-confined growth of the metal–organic framework HKUST-1. *Adv. Funct. Mater.* **32**, 2204065.

[76] Álvarez J R, Sánchez-González E, Pérez E, Schneider-Revueltas E, Martínez A, Tejeda-Cruz A, Islas-Jácome A, González-Zamora E and Ibarra I A. 2017. Structure stability of HKUST-1 towards water and ethanol and their effect on its CO_2 capture properties. *Dalton Trans.* **46**, 9192–9200.

[77] Yuan H Y, Tao J, Li N, Karmakar A, Tang C, Cai H, Pennycook S J, Singh N and Zhao D. 2019. On-chip tailorability of capacitive gas sensors integrated with metal–organic framework films. *Angew. Chem., Int. Ed.* **58**, 14089–14094.

[78] Mukherjee S, Manna B, Desai A V, Yin Y F, Krishna R, Babarao R and Ghosh S K. 2016. Harnessing Lewis acidic open metal sites of metal–organic frameworks: the foremost route to achieve highly selective benzene sorption over cyclohexane. *Chem. Commun.* **52**, 8215–8218.

[79] Ahmed I and Jhung S H. 2017. Applications of metal-organic frameworks in adsorption/separation processes via hydrogen bonding interactions. *Chem. Eng. J.* **310**, 197–215.

[80] Dalstein O, Ceratti D R, Boissière C, Grosso D, Cattoni A and Faustini M. 2016. Nanoimprinted, submicrometric, MOF-based 2D photonic structures: toward easy selective vapors sensing by a smartphone camera. *Adv. Funct. Mater.* **26**, 81–90.

[81] Lv Y Q, Xu P C, Yu H T, Xu J Q and Li X X. 2018. Ni-MOF-74 as sensing material for resonant-gravimetric detection of ppb-level CO. *Sens. Actuators B* **262**, 562–569.

[82] McGinn C K, Lamport Z A and Kymissis I. 2020. Review of gravimetric sensing of volatile organic compounds. *ACS Sens.* **5**, 1514–1534.

[83] Bloch E D et al. 2014. Reversible CO binding enables tunable CO/H_2 and CO/N_2 separations in metal–organic frameworks with exposed divalent metal cations. *J. Am. Chem. Soc.* **136**, 10752–10761.

[84] Cai S R, Li W, Xu P C, Xia X Y, Yu H T, Zhang S and Li X X. 2019. *In situ* construction of metal–organic framework (MOF) UiO-66 film on parylene-patterned resonant microcantilever for trace organophosphorus molecules detection. *Analyst* **144**, 3729–3735.

[85] Wang G et al. 2017. *Mechanism and kinetics for reaction of the chemical warfare agent simulant, DMMP(g)*, with zirconium(IV) MOFs: an ultrahigh-vacuum and DFT study. *J. Phys. Chem. C* **121**, 11261–11272.

[86] Tchalala M R et al. 2019. Fluorinated MOF platform for selective removal and sensing of SO_2 from flue gas and air. *Nat. Commun.* **10**, 1328.

[87] Zhang D, Fan Y, Li G, Du W, Li R, Liu Y, Cheng Z and Xu J. 2020. Biomimetic synthesis of zeolitic imidazolate frameworks and their application in high performance acetone gas sensors. *Sens. Actuators B* **302**, 127187.

[88] Hwang Y, Sohn H, Phan A, Yaghi O M and Candler R N. 2013. Dielectrophoresis-assembled zeolitic imidazolate framework nanoparticle-coupled resonators for highly sensitive and selective gas detection. *Nano Lett.* **13**, 5271–5276.

[89] Banerjee R, Phan A, Wang B, Knobler C, Furukawa H, O'Keeffe M and Yaghi O M. 2008. High-throughput synthesis of zeolitic imidazolate frameworks and application to CO_2 capture. *Science* **319**, 939–943.

[90] Liu Y Y, Hu E P, Khan E A and Lai Z P. 2010. Synthesis and characterization of ZIF-69 membranes and separation for CO_2/CO mixture. *J. Membr. Biol.* **353**, 36–40.

[91] Paschke B, Wixforth A, Denysenko D and Volkmer D. 2017. Fast surface acoustic wave-based sensors to investigate the kinetics of gas uptake in ultra-microporous frameworks. *ACS Sens.* **2**, 740–747.

[92] Zhu C, Perman J A, Gerald I I R E, Ma S Q and Huang J. 2019. Chemical detection using a metal–organic framework single crystal coupled to an optical fiber. *ACS Appl. Mater. Interfaces* **11**, 4393–4398.

[93] Blatov V A, Shevchenko A P and Proserpio D M. 2014. Applied topological analysis of crystal structures with the program package ToposPro. *Cryst. Growth Des.* **14**, 3576–3586.

[94] Kim K-J, Lu P, Culp J T and Ohodnicki P R. 2018. Metal–organic framework thin film coated optical fiber sensors: a novel waveguide-based chemical sensing platform. *ACS Sens.* **3**, 386–394.

[95] Phan-Quang G C et al. 2019. Tracking airborne molecules from afar: three-dimensional metal–organic framework-surface-enhanced raman scattering platform for stand-off and real-time atmospheric monitoring. *ACS Nano* **13**, 12090–12099.

[96] Yin H, Kim H, Choi J and Yip A C K. 2015. Thermal stability of ZIF-8 under oxidative and inert environments: a practical perspective on using ZIF-8 as a catalyst support. *Chem. Eng. J.* **278**, 293–300.

[97] Karnati P, Akbar S and Morris P A. 2019. Conduction mechanisms in one dimensional core-shell nanostructures for gas sensing: a review. *Sens. Actuators B* **295**, 127–143.
[98] Yuan H Y et al. 2019. ZnO nanosheets abundant in oxygen vacancies derived from metal-organic frameworks for ppb-level gas sensing. *Adv. Mater.* **31**, 1807161.
[99] Xia Y, Pan A F, Gardner D W, Zhao S K, Davey A K, Li Z, Zhao L B, Carraro C and Maboudian R. 2021. Well-connected ZnO nanoparticle network fabricated by in-situ annealing of ZIF-8 for enhanced sensitivity in gas sensing application. *Sens. Actuators B* **344**, 130180.
[100] Ren X W, Xu Z, Liu D, Li Y T, Zhang Z T and Tang Z L. 2022. Conductometric NO_2 gas sensors based on MOF-derived porous ZnO nanoparticles. *Sens. Actuators B* **357**, 131384.
[101] Koo W-T, Choi S-J, Kim S-J, Jang J-S, Tuller H L and Kim I-D. 2016. Heterogeneous sensitization of metal-organic framework driven metal@metal oxide complex catalysts on an oxide nanofiber scaffold toward superior gas sensors. *J. Am. Chem. Soc.* **138**, 13431–13437.
[102] Koo W-T, Cha J-H, Jung J-W, Choi S-J, Jang J-S, Kim D-H and Kim I-D. 2018. Few-layered WS_2 nanoplates confined in Co, N-doped hollow carbon nanocages: abundant WS_2 edges for highly sensitive gas sensors. *Adv. Funct. Mater.* **28**, 1802575.
[103] Min H, Kwon O, Lee J, Choi E, Kim J, Lee N, Eum K, Lee K H, Kim D W and Lee W. 2024. N-carbon-doped binary nanophase of metal oxide/metal–organic framework for extremely sensitive and selective gas response. *Adv. Mater.* **36**, 2309041.
[104] Jung H, Min H, Hwang J, Kim J, Choe Y-S, Lee H-S and Lee W. 2022. Selective detection of sub-1-ppb level isoprene using Pd-coated In_2O_3 thin film integrated in portable gas chromatography. *Appl. Surf. Sci.* **586**, 152827.
[105] Sun Y Y, Fan H Q, Shang Y Y, Lei L, Zhu S, Wang H, Dong W Q, Al-Bahrani M, Wang W J and Ma L T. 2023. MOF-5 derived 3D ZnO/Ag micro-octahedra for ultrahigh response and selective triethylamine detection at low temperature. *Sens. Actuators B* **390**, 133975.
[106] Bae J, Choi J S, Hwang S, Yun W S, Song D, Lee J and Jeong N C. 2017. Multiple coordination exchanges for room-temperature activation of open-metal sites in metal–organic frameworks. *ACS Appl. Mater. Interfaces*. **9**, 24743–24752.
[107] Li J-R, Sculley J and Zhou H-C. 2012. Metal–organic frameworks for separations. *Chem. Rev.* **112**, 869–932.
[108] Wang C, Liu D M and Lin W B. 2013. Metal–organic frameworks as a tunable platform for designing functional molecular materials. *J. Am. Chem. Soc.* **135**, 13222–13234.
[109] Lee J, Lee H, Bae T-H, Cho D, Choi M, Bae G, Shim Y-S and Jeon S. 2024. 3D ZnO/ZIF-8 hierarchical nanostructure for sensitive and selective NO_2 sensing at room temperature. *Small Struct.* **5**, 2300503.
[110] Yu B, Wang F F, Dong W B, Hou J, Lu P C and Gong J B. 2015. Self-template synthesis of core–shell ZnO@ZIF-8 nanospheres and the photocatalysis under UV irradiation. *Mater. Lett.* **156**, 50–53.
[111] Tian H L, Fan H Q, Li M M and Ma L T. 2016. Zeolitic imidazolate framework coated ZnO nanorods as molecular sieving to improve selectivity of formaldehyde gas sensor. *ACS Sens.* **1**, 243–250.
[112] Yao M-S, Tang W-X, Wang G-E, Nath B and Xu G. 2016. MOF thin film-coated metal oxide nanowire array: significantly improved chemiresistor sensor performance. *Adv. Mater.* **28**, 5229–5234.
[113] Wu X N, Xiong S, Gong Y, Gong Y, Wu W, Mao Z, Liu Q, Hu S and Long X. 2019. MOF-SMO hybrids as a H_2S sensor with superior sensitivity and selectivity. *Sens. Actuators B* **292**, 32–39.
[114] Zhou T T, Chen S Y, Wang X X, Xie C S and Zeng D W. 2020. Catalytic activation of cobalt doping sites in ZIF-71-coated ZnO nanorod arrays for enhancing gas-sensing performance to acetone. *ACS Appl. Mater. Interfaces* **12**, 48948–48956.
[115] Zhao Q, Ge Y L, Fu K X, Ji N, Song C F and Liu Q L. 2018. Oxidation of acetone over Co-based catalysts derived from hierarchical layer hydrotalcite: influence of Co/Al molar ratios and calcination temperatures. *Chemosphere* **204**, 257–266.
[116] Dmello M E, Sundaram N G and Kalidindi S B. 2018. Assembly of ZIF-67 metal–organic framework over tin oxide nanoparticles for synergistic chemiresistive CO_2 gas sensing. *Chem. Eur. J.* **24**, 9220–9223.
[117] Cho K H, Yoon J W, Lee J H, Kim J C, Kim K, Lee U-H, Kwak S K and Chang J-S. 2020. Effect of framework rigidity in metal-organic frameworks for adsorptive separation of ethane/ethylene. *Microporous Mesoporous Mater.* **307**, 110473.
[118] Kwon H T, Jeong H-K, Lee A S, An H S and Lee J S. 2015. Heteroepitaxially grown zeolitic imidazolate framework membranes with unprecedented propylene/propane separation performances. *J. Am. Chem. Soc.* **137**, 12304–12311.
[119] Hillman F, Brito J and Jeong H-K. 2018. Rapid one-pot microwave synthesis of mixed-linker hybrid zeolitic-imidazolate framework membranes for tunable gas separations. *ACS Appl. Mater. Interfaces* **10**, 5586–5593.
[120] Weber M, Kim J-H, Lee J-H, Kim J-Y, Iatsunskyi I, Coy E, Drobek M, Julbe A, Bechelany M and Kim S S. 2018. High-performance nanowire hydrogen sensors by exploiting the synergistic effect of Pd nanoparticles and metal–organic framework membranes. *ACS Appl. Mater. Interfaces* **10**, 34765–34773.
[121] Hwang K, Ahn J, Cho I, Kang K, Kim K, Choi J, Polychronopoulou K and Park I. 2020. Microporous elastomer filter coated with metal organic frameworks for improved selectivity and stability of metal oxide gas sensors. *ACS Appl. Mater. Interfaces* **12**, 13338–13347.
[122] Yamazoe N and Shimanoe K. 2013. 1—Fundamentals of semiconductor gas sensors. *In Semiconductor Gas Sensors* (eds Jaaniso R, Tan O K) (Woodhead Publishing, Oxford)
[123] Postica V et al. 2021. Improved long-term stability and reduced humidity effect in gas sensing: siO_2 ultra-thin layered ZnO columnar films. *Adv. Mater. Technol.* **6**, 2001137.
[124] Mahdavi H, Rahbarpour S, Hosseini-Golgoo S-M and Jamaati H. 2021. Reducing the destructive effect of ambient humidity variations on gas detection capability of a temperature modulated gas sensor by calcium chloride. *Sens. Actuators B* **331**, 129091.
[125] Qu F D, Zhang S, Huang C, Guo X, Zhu Y, Thomas T, Guo H, Attfield J P and Yang M. 2021. Surface functionalized sensors for humidity-independent gas detection. *Angew. Chem., Int. Ed.* **60**, 6561–6566.
[126] Tao Y, Yang B G, Wang F Y, Yan Y H, Hong X Y, Xu H H, Xia M Z and Wang F Y. 2022. Green synthesis of MOF-808 with modulation of particle sizes and defects for efficient phosphate sequestration. *Sep. Purif. Technol.* **300**, 121825.
[127] Bhakat P, Nigam A and Jagtap S. 2023. Green synthesis of MOF nanostructures: environmental benefits and applications. *Nanotechnol. Environ. Eng.* **8**, 815–827.
[128] Grande C A, Blom R, Spjelkavik A, Moreau V and Payet J. 2017. Life-cycle assessment as a tool for eco-design of metal-organic frameworks (MOFs). *Sustain. Mater. Technol.* **14**, 11–18.
[129] He C S, Zhang C W, Bian T F, Jiao K X, Su W K, Wu K-J and Su A. 2023. A review on artificial intelligence enabled

design, synthesis, and process optimization of chemical products for industry 4.0. *Processes* **11**, 330.

[130] Lai N S, Tew Y S, Zhong X L, Yin J, Li J L, Yan B H and Wang X N. 2023. Artificial intelligence (AI) workflow for catalyst design and optimization. *Ind. Eng. Chem. Res.* **62**, 17835–17848.

[131] Tian X L et al. 2024. Crosslinking-induced patterning of MOFs by direct photo- and electron-beam lithography. *Nat. Commun.* **15**, 2920.

[132] Falcaro P, Buso D, Hill A J and Doherty C M. 2012. Patterning techniques for metal organic frameworks. *Adv. Mater.* **24**, 3153–3168.

[133] Falcaro P, Ricco R, Doherty C M, Liang K, Hill A J and Styles M J. 2014. MOF positioning technology and device fabrication. *Chem. Soc. Rev.* **43**, 5513–5560.

[134] Jo Y-M, Kim D-H, Wang J D, Oppenheim J J and Dincă M. 2024. Humidity-mediated dual ionic-electronic conductivity enables high sensitivity in MOF chemiresistors. *J. Am. Chem. Soc.* **146**, 20213–20220.

[135] Ma Z H, Zhang Y, Xue Z, Fan Y, Wang L, Wang H, Zhong A and Xu J. 2024. Thermodynamically and kinetically enhanced benzene vapor sensor based on the Cu-TCPP-Cu MOF with extremely low limit of detection. *ACS Sens.* **9**, 1906–1915.

[136] Small L J, Hill R C, Krumhansl J L, Schindelholz M E, Chen Z H Y, Chapman K W, Zhang X R, Yang S H, Schröder M and Nenoff T M. 2019. Reversible MOF-based sensors for the electrical detection of iodine gas. *ACS Appl. Mater. Interfaces* **11**, 27982–27988.

[137] Noh H-J, Pennington D L, Seo J-M, Cline E, Benedetto G, Baek J-B, Hendon C H and Mirica K A. 2025. Reversible and ultrasensitive detection of nitric oxide using a conductive two-dimensional metal–organic framework. *Angew. Chem., Int. Ed.* **64**, e202419869.

[138] Park C, Shin H, Jeon M, Cho S H, Kim J and Kim I D. 2024. Single-atom catalysts in conductive metal-organic frameworks: enabling reversible gas sensing at room temperature. *ACS Nano* **18**, 26066–26075.